

Ground state and optical conductivity of interacting polarons in a quantum dot

S. N. Klimin*, V. M. Fomin*,**, F. Brosens, and J. T. Devreese**

*Theoretische Fysica van de Vaste Stoffen (TFVS),
Universiteit Antwerpen, B-2610 Antwerpen, Belgium*

(Dated: May 21, 2004)

Abstract

The ground-state energy, the addition energies and the optical absorption spectra are derived for interacting polarons in parabolic quantum dots in three and two dimensions. A path integral formalism for identical particles is used in order to take into account the fermion statistics. The approach is applied to both closed-shell and open-shell systems of interacting polarons. Using a generalization of the Jensen-Feynman variational principle, the ground-state energy of a confined N -polaron system is analyzed as a function of N and of the electron-phonon coupling constant α . As distinct from the few-electron systems without the electron-phonon interaction, *three* types of spin polarization are possible for the ground state of the few-polaron systems: (i) a spin-polarized state, (ii) a state where the spin is determined by Hund's rule, (iii) a state with the minimal possible spin. A transition from a state fulfilling Hund's rule, to a spin-polarized state occurs when decreasing the electron density. In the strong-coupling limit, the system of interacting polarons turns into a state with the minimal possible spin. These transitions should be experimentally observable in the optical absorption spectra of quantum dots.

I. INTRODUCTION

Many-electron states in quantum dots have been theoretically investigated by various approaches, e.g., the Hartree-Fock method [1, 2, 3], the density-functional theory [4, 5, 6, 7, 8, 9, 10], the quantum Monte Carlo simulation [11], the variational Monte Carlo method and the Padé approximation [12, 13], a numerical diagonalization of the Hamiltonian in a finite-dimensional basis [14]. The electron-phonon interaction was not taken into account in these investigations, although it can contribute significantly to both equilibrium and non-equilibrium properties of quantum dots. For instance, the effects due to the electron-phonon interaction play a key role in the optical spectra of some quantum dots (see Ref. [15] and references therein). Some characteristics revealed in the mid-infrared region of the experimentally observed optical absorption spectra of high- T_c cuprates [16, 17, 18, 19, 20] were assigned [21] to the polaron optical absorption at intermediate values of the electron-phonon coupling constant α . The infrared optical absorption band in the neodymium-cerium cuprate $\text{Nd}_{2-x}\text{Ce}_x\text{CuO}_{4-y}$ (NCCO), which was studied experimentally [22] as a function of the electron density, has been associated with the polaron optical absorption. Also some peculiarities of the infrared optical absorption spectra of cuprates and $\text{Pr}_2\text{NiO}_{4.22}$ were interpreted in terms of a mixture of large and small polarons or bipolarons [23, 24].

The theory of the optical conductivity of arbitrary-coupling single polarons has been developed in Refs. [25, 26] (see also the review [27] and references therein) within the memory-function method based on the path-integral formalism [28]. Recently, the optical absorption of a gas of interacting polarons at weak coupling was investigated [29, 30] on the basis of a variational many-particle approach [31]. The optical absorption of interacting polarons in bulk semiconductors at arbitrary coupling strength has been treated in Ref. [32] within the random-phase approximation, using variational parameters obtained from Feynman's *single-polaron* model [28], but this treatment does not seem to be a self-consistent approach to the many-polaron problem.

In contrast to the polaron mechanism of optical absorption in bulk (see Refs. [27, 33] and references therein), the polaron optical absorption in quantum dots, to the best of our knowledge, has not yet been widely studied. In order to investigate the ground state and the optical response of a system of interacting polarons in a quantum dot, it is crucial to take into account the fact that the system contains a *finite* number of identical particles (electrons or holes). Indeed, the thermodynamic properties of systems with a finite number of identical particles might substantially deviate from those obtained within the grand-canonical formalism (see, e.g., [34, 35]). The variational path-integral method for identical particles [34, 35, 36, 37] provides a useful tool for investigating interacting quantum many-body systems with a fixed (few or many) number of N particles. An outline of the method is given in Ref. [38], where we sketched the calculation of the ground-state energy of a fixed number of interacting polarons, which form a closed-shell system in a quantum dot.

In the present paper the calculation of the ground state and of the optical conductivity is performed for both closed-shell and open-shell systems of interacting polarons in a quantum dot. In Section II, we derive an upper bound to the free energy of a finite number of interacting polarons confined in a parabolic quantum dot in three dimensions and in two dimensions. In Section III we discuss the numerical results for the ground-state energy and for the addition energy of this system. In Section IV, the optical conductivity of interacting polarons in a quantum dot is derived on the basis of the memory-function method. The numerical results for the optical conductivity are discussed in Section V. The last section

VI contains conclusions.

II. THE PARTITION FUNCTION AND THE FREE ENERGY OF A MANY-POLARON SYSTEM

A. Interacting polarons in a quantum dot

We consider a system of N electrons with mutual Coulomb repulsion and interacting with the lattice vibrations. The system is assumed to be confined by a parabolic potential characterized by the frequency parameter Ω_0 . The total number of electrons is represented as $N = \sum_{\sigma} N_{\sigma}$, where N_{σ} is the number of electrons with the spin projection $\sigma = \pm 1/2$. The electron 3D (2D) coordinates are denoted by $\mathbf{x}_{j,\sigma}$ with $j = 1, \dots, N_{\sigma}$. The bulk phonons (characterized by 3D wave vectors \mathbf{q} and frequencies $\omega_{\mathbf{q}}$) are described by the complex coordinates $Q_{\mathbf{q}}$, which possess the property [39]

$$Q_{\mathbf{q}}^* = Q_{-\mathbf{q}}. \quad (1)$$

The full set of the electron and phonon coordinates are denoted by $\bar{\mathbf{x}} \equiv \{\mathbf{x}_{j,\sigma}\}$ and $\bar{Q} \equiv \{Q_{\mathbf{q}}\}$.

Throughout the sections II and III, the Euclidean time variable $\tau = it$ is used, where t is the real time variable. In this representation the Lagrangian of the system is

$$L(\dot{\bar{\mathbf{x}}}, \dot{\bar{Q}}; \bar{\mathbf{x}}, \bar{Q}) = L_e(\dot{\bar{\mathbf{x}}}, \bar{\mathbf{x}}) - V_C(\bar{\mathbf{x}}) + L_{ph}(\dot{\bar{Q}}, \bar{Q}) + L_{e-ph}(\bar{\mathbf{x}}, \bar{Q}), \quad (2)$$

where $L_e(\dot{\bar{\mathbf{x}}}, \bar{\mathbf{x}})$ is the Lagrangian of an electron with band mass m_b in a quantum dot:

$$L_e(\dot{\bar{\mathbf{x}}}, \bar{\mathbf{x}}) = - \sum_{\sigma=\pm 1/2} \sum_{j=1}^{N_{\sigma}} \left(\frac{m_b}{2} \dot{\mathbf{x}}_{j,\sigma}^2 + \frac{m_b}{2} \Omega_0^2 \mathbf{x}_{j,\sigma}^2 \right), \quad \dot{\mathbf{x}} \equiv \frac{d\mathbf{x}}{d\tau}, \quad (3)$$

$V_C(\bar{\mathbf{x}})$ is the potential energy of the electron-electron Coulomb repulsion in the medium with the high-frequency dielectric constant ε_{∞} :

$$V_C(\bar{\mathbf{x}}) = \sum_{\sigma, \sigma'=\pm 1/2} \sum_{j=1}^{N_{\sigma}} \sum_{l=1}^{N_{\sigma'}} \frac{e^2}{2\varepsilon_{\infty}} \frac{1}{|\mathbf{x}_{j,\sigma} - \mathbf{x}_{l,\sigma'}|}, \quad (j, \sigma) \neq (l, \sigma') \quad (4)$$

$L_{ph}(\dot{\bar{Q}}, \dot{\bar{Q}}^*; \bar{Q}, \bar{Q}^*)$ is the Lagrangian of free phonons:

$$L_{ph}(\dot{\bar{Q}}, \dot{\bar{Q}}^*; \bar{Q}, \bar{Q}^*) = -\frac{1}{2} \sum_{\mathbf{q}} (\dot{Q}_{\mathbf{q}}^* \dot{Q}_{\mathbf{q}} + \omega_{\mathbf{q}}^2 Q_{\mathbf{q}}^* Q_{\mathbf{q}}), \quad \dot{Q} \equiv \frac{dQ}{d\tau}. \quad (5)$$

Further, $L_{e-ph}(\bar{\mathbf{x}}, \bar{Q}, \bar{Q}^*)$ is the Lagrangian of the electron-phonon interaction:

$$L_{e-ph}(\bar{\mathbf{x}}, \bar{Q}) = - \sum_{\mathbf{q}} \left(\frac{2\omega_{\mathbf{q}}}{\hbar} \right)^{1/2} V_{\mathbf{q}} Q_{\mathbf{q}} \rho_{\mathbf{q}}, \quad (6)$$

where $\rho_{\mathbf{q}}$ is the Fourier transform of the electron density operator:

$$\rho_{\mathbf{q}} = \sum_{\sigma=\pm 1/2} \sum_{j=1}^{N_{\sigma}} e^{i\mathbf{q}\cdot\mathbf{x}_{j,\sigma}}. \quad (7)$$

$V_{\mathbf{q}}$ is the amplitude of the electron-phonon interaction. In this paper, we only consider electrons interacting with the long-wavelength longitudinal optical (LO) phonons with a dispersionless frequency $\omega_{\mathbf{q}} = \omega_{\text{LO}}$, for which the amplitude $V_{\mathbf{q}}$ is [26]

$$V_{\mathbf{q}} = \frac{\hbar\omega_{\text{LO}}}{q} \left(\frac{2\sqrt{2}\pi\alpha}{V} \right)^{1/2} \left(\frac{\hbar}{m_b\omega_{\text{LO}}} \right)^{1/4}, \quad (8)$$

where α is the electron-phonon coupling constant and V is the volume of the crystal.

We treat a *canonical* ensemble, where the numbers N_{σ} are fixed. The partition function $Z(\{N_{\sigma}\}, \beta)$ of the system can be expressed as a path integral over the electron and phonon coordinates:

$$Z(\{N_{\sigma}\}, \beta) = \sum_P \frac{(-1)^{\xi_P}}{N_{1/2}!N_{-1/2}!} \int d\bar{\mathbf{x}} \int_{\bar{\mathbf{x}}}^{P\bar{\mathbf{x}}} D\bar{\mathbf{x}}(\tau) \int d\bar{Q} \int_{\bar{Q}}^{\bar{Q}} D\bar{Q}(\tau) e^{-S[\bar{\mathbf{x}}(\tau), \bar{Q}(\tau)]}, \quad (9)$$

where $S[\bar{\mathbf{x}}(\tau), \bar{Q}(\tau)]$ is the “action” functional:

$$S[\bar{\mathbf{x}}(\tau), \bar{Q}(\tau)] = -\frac{1}{\hbar} \int_0^{\hbar\beta} L(\dot{\bar{\mathbf{x}}}, \dot{\bar{Q}}; \bar{\mathbf{x}}, \bar{Q}) d\tau. \quad (10)$$

The parameter $\beta \equiv 1/(k_B T)$ is inversely proportional to the temperature T . In order to take the Fermi-Dirac statistics into account, the integral over the electron paths $\{\bar{\mathbf{x}}(\tau)\}$ in Eq. (9) contains a sum over all permutations P of the electrons with the same spin projection, and ξ_P denotes the parity of a permutation P .

The action functional (10) is quadratic in the phonon coordinates \bar{Q} . Therefore, the path integral over the phonon variables in $Z(\{N_{\sigma}\}, \beta)$ can be calculated analytically [39]. As a result, the partition function of the electron-phonon system (9) factorizes into a product

$$Z(\{N_{\sigma}\}, \beta) = Z_p(\{N_{\sigma}\}, \beta) \prod_{\mathbf{q}} \frac{1}{2 \sinh(\beta \hbar \omega_{\text{LO}}/2)} \quad (11)$$

of the partition function of free phonons with a partition function $Z_p(\{N_{\sigma}\}, \beta)$ of interacting polarons, which is a path integral over the electron coordinates only:

$$Z_p(\{N_{\sigma}\}, \beta) = \sum_P \frac{(-1)^{\xi_P}}{N_{1/2}!N_{-1/2}!} \int d\bar{\mathbf{x}} \int_{\bar{\mathbf{x}}}^{P\bar{\mathbf{x}}} D\bar{\mathbf{x}}(\tau) e^{-S_p[\bar{\mathbf{x}}(\tau)]}. \quad (12)$$

The functional

$$\begin{aligned} S_p[\bar{\mathbf{x}}(\tau)] = & -\frac{1}{\hbar} \int_0^{\hbar\beta} [L_e(\dot{\bar{\mathbf{x}}}(\tau), \bar{\mathbf{x}}(\tau)) + V_C(\bar{\mathbf{x}}(\tau))] d\tau \\ & - \sum_{\mathbf{q}} \frac{|V_{\mathbf{q}}|^2}{2\hbar^2} \int_0^{\hbar\beta} d\tau \int_0^{\hbar\beta} d\tau' \frac{\cosh[\omega_{\text{LO}}(|\tau - \tau'| - \hbar\beta/2)]}{\sinh(\beta \hbar \omega_{\text{LO}}/2)} \rho_{\mathbf{q}}(\tau) \rho_{-\mathbf{q}}(\tau') \end{aligned} \quad (13)$$

results from the elimination of the phonon coordinates and contains the “influence phase” of the phonons (the last term in the right-hand side). It describes the phonon-induced retarded interaction between the electrons, including the retarded self-interaction of each electron. The free energy of a system of interacting polarons $F_p(\{N_\sigma\}, \beta)$ is related to their partition function (12) by the equation:

$$F_p(\{N_\sigma\}, \beta) = -\frac{1}{\beta} \ln Z_p(\{N_\sigma\}, \beta). \quad (14)$$

At present no method is known to calculate the non-gaussian path integral (12) analytically. For *distinguishable* particles, the Jensen-Feynman variational principle [39] provides a convenient approximation technique. It yields a lower bound to the partition function, and hence an upper bound to the free energy.

The formulation of a variational principle for the free energy for a system of *identical particles* is a non-trivial problem. However, it can be shown [36] that the path-integral approach to the many-body problem for a fixed number of identical particles can be formulated as a Feynman-Kac functional on a state space for N indistinguishable particles, by imposing an ordering on the configuration space and by the introduction of a set of boundary conditions at the boundaries of this state space. The path integral (in the imaginary-time variable) for identical particles was shown to be *positive* within this state space. This implies that a many-body extension of the Jensen-Feynman inequality was found, which can be used for interacting identical particles (Ref.[36], p. 4476). A more detailed analysis of this variational principle for both local and retarded interactions can be found in Ref. [37]. It is required that the potentials are symmetric with respect to all permutations of the particle positions, and that both the exact propagator and the model propagator are antisymmetric (for fermions) with respect to permutations of any two electrons at any moment in time. This means that these propagators have to be defined on the same configuration space. Keeping in mind these constraints, the variational inequality for identical particles takes the same form as the Jensen-Feynman variational principle:

$$F_p \leq F_0 + \frac{1}{\beta} \langle S_p - S_0 \rangle_{S_0}, \quad (15)$$

where S_0 is a model action with corresponding free energy F_0 . The angular brackets mean a weighted average over the paths

$$\langle (\bullet) \rangle_{S_0} = \frac{\sum_P \frac{(-1)^{\xi_P}}{N_{1/2}! N_{-1/2}!} \int d\bar{\mathbf{x}} \int_{\bar{\mathbf{x}}}^{P\bar{\mathbf{x}}} D\bar{\mathbf{x}}(\tau) (\bullet) e^{-S_0[\bar{\mathbf{x}}(\tau)]}}{\sum_P \frac{(-1)^{\xi_P}}{N_{1/2}! N_{-1/2}!} \int d\bar{\mathbf{x}} \int_{\bar{\mathbf{x}}}^{P\bar{\mathbf{x}}} D\bar{\mathbf{x}}(\tau) e^{-S_0[\bar{\mathbf{x}}(\tau)]}}. \quad (16)$$

B. Model system

We consider a model system consisting of N electrons with coordinates $\bar{\mathbf{x}} \equiv \{\mathbf{x}_{j,\sigma}\}$ and N_f fictitious particles with coordinates $\bar{\mathbf{y}} \equiv \{\mathbf{y}_j\}$ in a harmonic confinement potential with elastic interparticle interactions as studied in Ref. [38]. The Lagrangian of this model system

takes the form

$$\begin{aligned}
L_M(\dot{\bar{\mathbf{x}}}, \dot{\bar{\mathbf{y}}}; \bar{\mathbf{x}}, \bar{\mathbf{y}}) = & -\frac{m_b}{2} \sum_{\sigma} \sum_{j=1}^{N_{\sigma}} (\dot{\mathbf{x}}_{j,\sigma}^2 + \Omega^2 \mathbf{x}_{j,\sigma}^2) + \frac{m_b \omega^2}{4} \sum_{\sigma, \sigma'} \sum_{j=1}^{N_{\sigma}} \sum_{l=1}^{N_{\sigma'}} (\mathbf{x}_{j,\sigma} - \mathbf{x}_{l,\sigma'})^2 \\
& - \frac{m_f}{2} \sum_{j=1}^{N_f} (\dot{\mathbf{y}}_j^2 + \Omega_f^2 \mathbf{y}_j^2) - \frac{k}{2} \sum_{\sigma} \sum_{j=1}^{N_{\sigma}} \sum_{l=1}^{N_f} (\mathbf{x}_{j,\sigma} - \mathbf{y}_l)^2.
\end{aligned} \tag{17}$$

The frequencies Ω , ω , Ω_f , the mass of a fictitious particle m_f , and the force constant k are variational parameters. Clearly, this Lagrangian is symmetric with respect to electron permutations. Performing the path integral over the coordinates of the fictitious particles [39], the partition function $Z_0(\{N_{\sigma}\}, \beta)$ of the model system of interacting polarons becomes a path integral over the electron coordinates:

$$Z_0(\{N_{\sigma}\}, \beta) = \sum_P \frac{(-1)^{\xi_P}}{N_{1/2}! N_{-1/2}!} \int d\bar{\mathbf{x}} \int_{\bar{\mathbf{x}}}^{P\bar{\mathbf{x}}} D\bar{\mathbf{x}}(\tau) e^{-S_0[\bar{\mathbf{x}}(\tau)]}, \tag{18}$$

with the action functional $S_0[\bar{\mathbf{x}}(\tau)]$ given by

$$\begin{aligned}
S_0[\bar{\mathbf{x}}(\tau)] = & \frac{1}{\hbar} \int_0^{\hbar\beta} \sum_{\sigma} \sum_{j=1}^{N_{\sigma}} \frac{m_b}{2} [\dot{\mathbf{x}}_{j,\sigma}^2(\tau) + \Omega^2 \mathbf{x}_{j,\sigma}^2(\tau)] d\tau \\
& - \frac{1}{\hbar} \int_0^{\hbar\beta} \sum_{\sigma, \sigma'} \sum_{j=1}^{N_{\sigma}} \sum_{l=1}^{N_{\sigma'}} \frac{m_b \omega^2}{4} [\mathbf{x}_{j,\sigma}(\tau) - \mathbf{x}_{l,\sigma'}(\tau)]^2 d\tau \\
& - \frac{k^2 N^2 N_f}{4m_f \hbar \Omega_f} \int_0^{\hbar\beta} d\tau \int_0^{\hbar\beta} d\tau' \frac{\cosh[\Omega_f(|\tau - \tau'| - \hbar\beta/2)]}{\sinh(\beta \hbar \Omega_f/2)} \mathbf{X}(\tau) \cdot \mathbf{X}(\tau'),
\end{aligned} \tag{19}$$

where \mathbf{X} is the center-of-mass coordinate of the electrons,

$$\mathbf{X} = \frac{1}{N} \sum_{\sigma} \sum_{j=1}^{N_{\sigma}} \mathbf{x}_{j,\sigma}. \tag{20}$$

The details of the analytical calculation of the model partition function (18) are described in Appendix A.

After substituting the model action functional (19) into the right-hand side of the varia-

tional inequality (15), we obtain an upper bound to the free energy F_{var} ,

$$\begin{aligned}
& F_{var}(\{N_\sigma\}, \beta) \\
&= F_0(\{N_\sigma\}, \beta) + \frac{m_b}{2} (\Omega_0^2 - \Omega^2 + N\omega^2) \left\langle \sum_{j=1}^N \mathbf{x}_j^2(0) \right\rangle_{S_0} \\
&\quad - \frac{m_b \omega^2 N^2}{2} \langle \mathbf{X}^2(0) \rangle_{S_0} + \sum_{\mathbf{q} \neq 0} \frac{2\pi e^2}{V \varepsilon_\infty q^2} [g(\mathbf{q}, 0 | \{N_\sigma\}, \beta) - N] \\
&\quad + \frac{k^2 N^2 N_f}{4m_f \beta \hbar \Omega_f} \int_0^{\hbar\beta} d\tau \int_0^{\hbar\beta} d\tau' \frac{\cosh[\Omega_f(|\tau - \tau'| - \hbar\beta/2)]}{\sinh(\beta \hbar \Omega_f/2)} \langle \mathbf{X}(\tau) \cdot \mathbf{X}(\tau') \rangle_{S_0} \\
&\quad - \sum_{\mathbf{q}} \frac{|V_{\mathbf{q}}|^2}{2\hbar^2 \beta} \int_0^{\hbar\beta} d\tau \int_0^{\hbar\beta} d\tau' \frac{\cosh[\omega_{LO}(|\tau - \tau'| - \hbar\beta/2)]}{\sinh(\beta \hbar \omega_{LO}/2)} g(\mathbf{q}, \tau - \tau' | \{N_\sigma\}, \beta). \quad (21)
\end{aligned}$$

Here, $g(\mathbf{q}, \tau - \tau' | \{N_\sigma\}, \beta)$ is the two-point correlation function for the electron density operators:

$$g(\mathbf{q}, \tau | \{N_\sigma\}, \beta) = \langle \rho_{\mathbf{q}}(\tau) \rho_{-\mathbf{q}}(0) \rangle_{S_0}. \quad (22)$$

Both the free energy and the correlation functions of the model system can be calculated analytically using the generating function technique [34]. In the zero-temperature limit ($\beta \rightarrow \infty$), the variational free energy (21) becomes an upper bound $E_{var}^0(\{N_\sigma\})$ to the ground-state energy E^0 of the system of interacting polarons. The details of the calculation of the correlation functions are given in the Appendix B.

III. GROUND-STATE ENERGY AND ADDITION ENERGY OF INTERACTING POLARONS

For the numerical calculations, we use effective atomic units, where \hbar , the electron band mass m_b and $e/\sqrt{\varepsilon_\infty}$ have the numerical value of 1. This means that the unit of length is the effective Bohr radius $a_B^* = \hbar^2 \varepsilon_\infty / (m_b e^2)$, while the unit of energy is the effective Hartree[14] $H^* = m_b e^4 / (\hbar^2 \varepsilon_\infty^2)$. These units allow to present results for quantum dots with and without the electron-phonon interaction on the same scale. Therefore, for confined polarons they are more convenient than the usual polaron units, where the unit of length is $a_p \equiv [\hbar / (m_b \omega_{LO})]^{1/2}$, and the energy is measured in units of the LO-phonon energy $\hbar \omega_{LO}$. In terms of the dimensionless parameters α and $\eta \equiv \varepsilon_\infty / \varepsilon_0$, where ε_0 is the static dielectric constant, the following relations exist between both systems of units:

$$\frac{a_p}{a_B^*} = \frac{\sqrt{2}\alpha}{1-\eta}, \quad \frac{H^*}{\hbar \omega_{LO}} = \left(\frac{a_p}{a_B^*} \right)^2 = \frac{2\alpha^2}{(1-\eta)^2}. \quad (23)$$

In Fig. 1, the total spin S of a system of interaction polarons in their ground state is plotted as a function of the number of electrons in a 3D quantum dot for different values of the confinement frequency Ω_0 , of the electron-phonon coupling constant α and of the parameter η . As distinct from few-electron systems without the electron-phonon interaction, three types of spin polarization are possible for the ground state, which should be distinguishable from each other using, e.g., capacity measurements.

(i) Except for the strong-coupling case and for the low-density case, the filling in the ground state is as follows: in an open shell, with less-than-half filling, each new electron is added with one and the same spin, so that the total spin (in the shell under consideration) is maximal in accordance with Hund's rule [40]. As soon as half-filling is achieved with electrons possessing a certain spin, each new electron is added with the spin opposite to that in the group of electrons providing the aforementioned half-filling. When the number of electrons corresponds to the number of states in the shell under consideration, the shell becomes closed, and the total spin is zero. This mode of filling is referred to as Hund's rule for a quantum dot. Hund's rule means, that the electrons in a partly filled upper shell build up a minimal possible number of pairs in order to minimize the electron-electron repulsion. For a quantum dot with $\hbar\Omega_0 = 0.5 H^*$ at $\alpha = 0$ and at $\alpha = 0.5$, the shell filling always obeys Hund's rule, as shown in Fig. 1(a).

(ii) With decreasing confinement frequency Ω_0 at a given number of electrons, the electron density lowers. For densities smaller than a certain value, it can happen that the ground state is a state with a maximal total (in all shells) spin. In this state, the electrons are filling consecutively all the single-electron states with one and the same spin and are referred to as spin-polarized. The examples are the states at $\alpha = 0$ for $N = 4$ and $N = 10$ in Fig. 1(b). A spin-polarized ground state precedes the formation of a Wigner crystal when further lowering the density [14, 41].

(iii) In the strong-coupling case ($\alpha \gg 1$ and $\eta \ll 1$), it can happen that the ground state is a state with a minimal total spin (0 for even number of electrons and $\frac{1}{2}$ for odd number of electrons). This is the case when –due to the phonon-mediated electron-electron attraction– pairing of electrons with opposite spins occurs, analogous to a singlet bipolaron ground state in bulk. The examples are the states at $\alpha = 5$ and $\eta = 0.1$ for N in the range from 4 to 6 in Fig. 1(a) and for N in the range from 4 to 10 in Fig. 1(b). This trend to minimize the total spin is a consequence of the electron-phonon interaction, presumably due to the fact that the phonon-mediated electron-electron attraction overcomes the Coulomb repulsion. With an increasing number of electrons, at a certain value of N , such states with a minimal total spin cease to form the ground state, and the shell filling abruptly returns to that prescribed by Hund's rule [see a jump in the spin at $\alpha = 5$ when N changes from 10 to 11 in Fig. 1(b)]. This jump is analogous to a transition from states with paired electrons (like superconducting states) to another type of states with unpaired electrons (like normal states).

The addition energy $\Delta(N)$, which is the variation of the chemical potential when putting an extra electron into a quantum dot, is defined as [4, 5]

$$\Delta(N) = E^0(N+1) - 2E^0(N) + E^0(N-1). \quad (24)$$

Fig. 2 presents the addition energy in a 3D quantum dot as a function of the number of electrons. The structure of $\Delta(N)$ clearly manifests the shell structure of a quantum dot. The most pronounced peaks in the addition energy occur for closed-shell systems with $N = 2, 8, 20$. The peaks in $\Delta(N)$ at $N = 5$ and $N = 14$ obtained within the present approach for relatively weak electron-phonon coupling correspond to the systems with the half-filled upper shell (see Fig. 2(a) for $\alpha = 0$ and $\alpha = 0.5$). In these cases the total spin for the upper shell takes its maximal possible value, in accordance with Hund's rule. At sufficiently large values of α , the electron-phonon interaction substantially modifies the addition energy. In the strong-coupling case, the peaks corresponding to half-filled shells become less pronounced, while those corresponding to closed-shell systems become more prominent as compared to the weak-coupling case.

To the best of our knowledge, the addition energy for parabolic quantum dots was obtained using the density functional theory (DFT) (see, e.g., Refs.[4, 5, 8]) only without the electron-phonon interaction. Our results for the addition energy for a 3D quantum dot as a function of N in the particular case $\alpha = 0$ are very close for $N \leq 12$ to those calculated within the DFT [8] with an optimized effective potential and a self-interaction correction [42].

The panels *a* and *b* in Fig. 3 represent, respectively, the total spin and the addition energy for interacting polarons in a 2D parabolic GaAs quantum dot with the confinement parameter $\hbar\Omega_0 = 0.5 H^* \approx 7.67$ meV. The pronounced peaks in $\Delta(N)$ at $N = 2, 6, 12, 20, \dots$ correspond to the closed-shell systems, for which the total spin equals zero. In accordance with Hund's rule, the upper shell is filled in such a way that the total spin of electrons in this shell takes the maximal possible value. Therefore for the half-filled upper shell (at $N = 4, 9, 16, \dots$) maxima of the total spin occur as a function of N . At these electron numbers, the addition energy manifests peaks, which are less pronounced than those corresponding to closed shells.

The inset to Fig. 3(*b*) shows the experimental data for the addition energy in a cylindric GaAs quantum dot [43]. As seen from Fig. 3, the peak positions for the addition energy of interacting polarons in a 2D parabolic quantum dot agree well with the experimental results for the addition energies of cylindrical quantum dots. The height of the calculated peaks of the addition energy falls down as the shell number increases, which is qualitatively consistent with the experimentally observed behavior [43]. The peaks in $\Delta(N)$ corresponding to the half-filled shells are weaker than those for the closed shells both in the experiment[43] and in our theory.

IV. OPTICAL CONDUCTIVITY

For a system of interacting polarons in a parabolic confinement potential, we calculate the real part of the optical conductivity within the memory-function approach. For a single polaron at arbitrary coupling strength it was developed in Refs. [25, 26]. For a polaron gas in the weak-coupling limit, this technique was applied in Ref. [44].

In the present paper we extend the memory-function approach to a system of arbitrary-coupling interacting polarons. Since the optical conductivity relates the current $\mathbf{J}(t)$ per electron to a time-dependent uniform electric field $\mathbf{E}(t)$ in the framework of linear response theory, we have to return to the *real-time* representation in the path integrals. The Fourier components of the electric field are denoted by \mathbf{E}_ω :

$$\mathbf{E}(t) = \frac{1}{2\pi} \int_{-\infty}^{\infty} \mathbf{E}_\omega e^{-i\omega t} d\omega, \quad (25)$$

and the similar denotations are used for other time-dependent quantities. The electric current per electron $\mathbf{J}(t)$ is related to the mean electron coordinate response $\mathbf{R}(t)$ by

$$\mathbf{J}(t) = -e \frac{d\mathbf{R}(t)}{dt}, \quad (26)$$

and hence

$$\mathbf{J}_\omega = i e \omega \mathbf{R}_\omega. \quad (27)$$

Within the linear-response theory, both the electric current and the coordinate response are proportional to \mathbf{E}_ω :

$$\mathbf{J}_\omega = \sigma(\omega) \mathbf{E}_\omega, \quad \mathbf{R}_\omega = \frac{\sigma(\omega)}{ie\omega} \mathbf{E}_\omega, \quad (28)$$

where $\sigma(\omega)$ is the conductivity per electron. Because we treat an isotropic electron-phonon system, $\sigma(\omega)$ is a scalar function. It is determined from the time evolution of the center-of-mass coordinate:

$$\mathbf{R}(t) \equiv \frac{1}{N} \left\langle \left\langle \sum_{j=1}^N \mathbf{x}_j(t) \right\rangle \right\rangle_S. \quad (29)$$

The symbol $\langle\langle(\bullet)\rangle\rangle_S$ denotes an average in the *real-time* representation for a system with action functional S :

$$\langle\langle(\bullet)\rangle\rangle_S \equiv \int d\bar{\mathbf{x}} \int d\bar{\mathbf{x}}_0 \int_{\bar{\mathbf{x}}_0}^{\bar{\mathbf{x}}} d\bar{\mathbf{x}}'_0 \int_{\bar{\mathbf{x}}'_0}^{\bar{\mathbf{x}}} D\bar{\mathbf{x}}(t) \int_{\bar{\mathbf{x}}'_0}^{\bar{\mathbf{x}}} D\bar{\mathbf{x}}'(t) e^{\frac{i}{\hbar} S[\bar{\mathbf{x}}(t), \bar{\mathbf{x}}'(t)]} (\bullet) \left\langle \bar{\mathbf{x}}_0 | \hat{\rho}(t_0) | \bar{\mathbf{x}}'_0 \right\rangle \Big|_{t_0 \rightarrow -\infty}, \quad (30)$$

where $\langle \bar{\mathbf{x}}_0 | \hat{\rho}(t_0) | \bar{\mathbf{x}}'_0 \rangle$ is the density matrix before the onset of the electric field in the infinite past ($t_0 \rightarrow -\infty$). The corresponding action functional is [45, 46]

$$S[\bar{\mathbf{x}}(t), \bar{\mathbf{x}}'(t)] = \int_{-\infty}^t \left[L_e(\dot{\bar{\mathbf{x}}}(t), \bar{\mathbf{x}}(t), t) - L_e(\dot{\bar{\mathbf{x}}}'(t), \bar{\mathbf{x}}'(t), t) \right] dt' - i\hbar \Phi[\bar{\mathbf{x}}(t), \bar{\mathbf{x}}'(t)], \quad (31)$$

where $L_e(\dot{\bar{\mathbf{x}}}, \bar{\mathbf{x}}, t)$ is the Lagrangian of N interacting electrons in a time-dependent uniform electric field $\mathbf{E}(t)$

$$L_e(\dot{\bar{\mathbf{x}}}, \bar{\mathbf{x}}, t) = \sum_{\sigma} \sum_{j=1}^{N_{\sigma}} \left(\frac{m_b \dot{\bar{\mathbf{x}}}_{j,\sigma}^2}{2} - \frac{m_b \Omega_0^2 \bar{\mathbf{x}}_{j,\sigma}^2}{2} - e \bar{\mathbf{x}}_{j,\sigma} \cdot \mathbf{E}(t) \right) - \sum_{\sigma, \sigma'} \sum_{j=1}^{N_{\sigma}} \sum_{l=1}^{N_{\sigma'}} \frac{e^2}{2\varepsilon_{\infty} |\bar{\mathbf{x}}_{j,\sigma} - \bar{\mathbf{x}}_{l,\sigma'}|}. \quad (32)$$

The influence phase of the phonons (see, e.g., Ref. [46])

$$\begin{aligned} \Phi[\bar{\mathbf{x}}(s), \bar{\mathbf{x}}'(s)] = & - \sum_{\mathbf{q}} \frac{|V_{\mathbf{q}}|^2}{\hbar^2} \int_{-\infty}^t ds \int_{-\infty}^s ds' [\rho_{\mathbf{q}}(s) - \rho'_{\mathbf{q}}(s)] \\ & \times \left[T_{\omega_{\mathbf{q}}}^*(s-s') \rho_{\mathbf{q}}(s') - T_{\omega_{\mathbf{q}}}(s-s') \rho'_{\mathbf{q}}(s') \right] \end{aligned} \quad (33)$$

describes both a retarded interaction between different electrons and a retarded self-interaction of each electron due to the elimination of the phonon coordinates. This functional contains the free-phonon Green's function:

$$T_{\omega}(t) = \frac{e^{i\omega t}}{1 - e^{-\beta\hbar\omega}} + \frac{e^{-i\omega t}}{e^{\beta\hbar\omega} - 1}. \quad (34)$$

The equation of motion for $\mathbf{R}(t)$ can be derived by analogy with that described in Ref. [47]:

$$m_b \frac{d^2 \mathbf{R}(t)}{dt^2} + m_b \Omega_0^2 \mathbf{R}(t) + e \mathbf{E}(t) = \mathbf{F}_{ph}(t), \quad (35)$$

where $\mathbf{F}_{ph}(t)$ is the average force due to the electron-phonon interaction,

$$\mathbf{F}_{ph}(t) = -\text{Re} \sum_{\mathbf{q}} \frac{2|V_{\mathbf{q}}|^2 \mathbf{q}}{N\hbar} \int_{-\infty}^t ds T_{\omega_{LO}}^*(t-s) \langle \langle \rho_{\mathbf{q}}(t) \rho_{-\mathbf{q}}(s) \rangle \rangle_S. \quad (36)$$

The two-point correlation function $\langle \langle \rho_{\mathbf{q}}(t) \rho_{-\mathbf{q}}(s) \rangle \rangle_S$ should be calculated from Eq. (30) using the exact action (31), but like for the free energy above, this path integral cannot be calculated analytically. Instead, we perform an approximate calculation, replacing the two-point correlation function in Eq. (36) by $\langle \langle \rho_{\mathbf{q}}(t) \rho_{-\mathbf{q}}(s) \rangle \rangle_{S_0}$, where $S_0[\bar{\mathbf{x}}(t), \bar{\mathbf{x}}'(t)]$ is the action functional with the optimal values of the variational parameters for the model system considered in the previous section in the presence of the electric field $\mathbf{E}(t)$. The functional $S_0[\bar{\mathbf{x}}(t), \bar{\mathbf{x}}'(t)]$ is quadratic and describes a system of coupled harmonic oscillators in the uniform electric field $\mathbf{E}(t)$. This field enters the term $-e\mathbf{E}(t) \cdot \sum_{\sigma} \sum_{j=1}^{N_{\sigma}} \mathbf{x}_{j,\sigma}$ in the Lagrangian, which only affects the center-of-mass coordinate. Hence, a shift of variables to the frame of reference with the origin at the center of mass

$$\begin{cases} \mathbf{x}_n(t) = \tilde{\mathbf{x}}_n(t) + \mathbf{R}(t), \\ \mathbf{x}'_n(t) = \tilde{\mathbf{x}}'_n(t) + \mathbf{R}(t), \end{cases} \quad (37)$$

results in [46]

$$\langle \langle \rho_{\mathbf{q}}(t) \rho_{-\mathbf{q}}(s) \rangle \rangle_{S_0} = \langle \langle \rho_{\mathbf{q}}(t) \rho_{-\mathbf{q}}(s) \rangle \rangle_{S_0} \Big|_{E=0} e^{i\mathbf{q} \cdot [\mathbf{R}(t) - \mathbf{R}(s)]}. \quad (38)$$

This result (38) is valid for any *quadratic* model action S_0 .

The applicability of the parabolic approximation for $N = 1$ is confirmed by the fact, that for the polaron ground-state energy, the results of the Feynman approach [28] are very close to the values obtained using other reliable methods [54, 55, 56, 57, 58]. Thus, a self-induced polaronic potential, created by the polarization cloud around an electron, is rather well described by a parabolic potential whose parameters are determined by a variational method. For $N = 2$, the lowest known values of the bipolaron ground-state energy are provided by the path-integral variational method with parabolic potentials both in bulk [59] and for confined systems [60, 61] for realistic values of α . The aforesaid approximation for the right-hand side of Eq. (36) is a direct generalization of the all-coupling approach [25, 46, 53] to a many-polaron system. For weak coupling, our variational method is at least of the same accuracy as the perturbation theory, which results from our approach at a special choice of the variational parameters. For strong coupling, an interplay of the electron-phonon interaction and the Coulomb correlations within a confinement potential can lead to the assemblage of polarons in multi-polaron systems. As shown in Refs. [60, 61] for a system with $N = 2$, the presence of a confinement potential strongly favors the bipolaron formation. Our choice of the model variational system is reasonable because of this trend, apparently occurring in a many-polaron system with arbitrary N for a finite confinement strength.

The correlation function $\langle \rho_{\mathbf{q}}(t) \rho_{-\mathbf{q}}(s) \rangle_{S_0} \Big|_{\mathbf{E}=0}$ corresponds to the model system in the absence of an electric field. For $t > s$, this function is related to the imaginary-time correlation function $g(\mathbf{q}, \tau | \{N_{\sigma}\}, \beta)$, described in the previous section:

$$\langle \langle \rho_{\mathbf{q}}(t) \rho_{-\mathbf{q}}(s) \rangle \rangle_{S_0} \Big|_{\mathbf{E}=0, t>s} = g(\mathbf{q}, i(t-s) | \{N_{\sigma}\}, \beta). \quad (39)$$

Using the transformation (37) and the relation (39), one readily obtains

$$\mathbf{F}_{ph}(t) = -\text{Re} \sum_{\mathbf{q}} \frac{2|V_{\mathbf{q}}|^2 \mathbf{q}}{N\hbar} \int_{-\infty}^t T_{\omega_{LO}}^*(t-s) e^{i\mathbf{q} \cdot [\mathbf{R}(t) - \mathbf{R}(s)]} g(\mathbf{q}, i(t-s) | \{N_{\sigma}\}, \beta) ds. \quad (40)$$

Within the framework of the linear-response theory, the external electric field $\mathbf{E}(t)$ is a small perturbation, so that $\mathbf{R}(t)$ is a linear functional of $[\mathbf{E}(t')]|_{t' \leq t}$. Expanding the function $e^{i\mathbf{q} \cdot [\mathbf{R}(t) - \mathbf{R}(s)]}$ in the right-hand side of Eq. (40) in powers of $[\mathbf{R}(t) - \mathbf{R}(s)]$ up to the first-order term, we obtain the Fourier component $\mathbf{F}_{ph}(\omega)$ of the force due to the electron-phonon interaction which is proportional to \mathbf{R}_{ω} . As a result, the optical conductivity can be expressed in terms of the memory function $\chi(\omega)$ (cf. Refs. [25, 26]),

$$\text{Re} \sigma(\omega) = -\frac{e^2}{m_b} \frac{\omega \text{Im} \chi(\omega)}{[\omega^2 - \Omega_0^2 - \text{Re} \chi(\omega)]^2 + [\text{Im} \chi(\omega)]^2}, \quad (41)$$

where $\chi(\omega)$ is given by

$$\chi(\omega) = \sum_{\mathbf{q}} \frac{2|V_{\mathbf{q}}|^2 q^2}{3N\hbar m_b} \int_0^{\infty} dt (e^{i\omega t} - 1) \text{Im} [T_{\omega_{LO}}^*(t) g(\mathbf{q}, it | \{N_{\sigma}\}, \beta)]. \quad (42)$$

It is worth noting that the optical conductivity (41) differs from that for a translationally invariant polaron system both by the explicit form of $\chi(\omega)$ and by the presence of the term Ω_0^2 in the denominator. For $\alpha \rightarrow 0$, the optical conductivity tends to a δ -like peak at $\omega = \Omega_0$,

$$\lim_{\alpha \rightarrow 0} \text{Re} \sigma(\omega) = \frac{\pi e^2}{2m_b} \delta(\omega - \Omega_0). \quad (43)$$

For a translationally invariant system $\Omega_0 \rightarrow 0$, and this weak-coupling expression (43) reproduces the “central peak” of the polaron optical conductivity [48].

In the zero-temperature limit, the memory function of Eq. (42) is derived in the analytical form of Eq. (B.15) in Appendix B for 3D and 2D interacting polarons.

V. RESULTS ON THE OPTICAL CONDUCTIVITY

Due to the confinement, the electron motion in a quantum dot is fully quantized. Hence, when a photon is absorbed, the electron recoil can be transferred only by discrete quanta. As a result, the optical conductivity spectrum of a system of interacting polarons in a quantum dot is a series of δ -like peaks as distinct from the optical conductivity spectrum of a bulk polaron [25, 26]. These peaks are related to the internal polaron excitations.

Because $\text{Im} \chi(\omega) = 0$ for all frequencies except for a discrete set of combinatorial frequencies (B.16), the peaks in the optical conductivity (41) are positioned at the frequencies which are given by the roots of the equation

$$\omega^2 - \Omega_0^2 - \text{Re} \chi(\omega) = 0, \quad (44)$$

which are denoted as $(\tilde{\Omega}_1, \tilde{\Omega}_2, \dots)$.

One of these roots is close to the variational parameter Ω_2 , which is the eigenfrequency of the motion of a polaron as a whole. It satisfies the inequality $\Omega_2 < \Omega_0$ because the polaron effective mass is larger than that of a bare electron. Ω_2 is close to Ω_0 in the weak-coupling case and decreases with increasing α . Hence, it tends to zero in the limit $\Omega_0 \rightarrow 0$. The peak in $\text{Re } \sigma(\omega)$ corresponding to this root can be considered as the *zero-phonon* line, which is an analogue of the “central peak” of the polaron optical conductivity [25, 26]. The peaks of $\text{Re } \sigma(\omega)$ determined by the other roots of Eq. (44) can be attributed to transitions into excited states of the many-polaron system.

The changes of the shell filling schemes, which occur when varying the confinement frequency, manifest themselves in the spectra of the optical conductivity. In Fig. 4, optical conductivity spectra for $N = 20$ polarons are presented for a quantum dot with the parameters of CdSe: $\alpha = 0.46$, $\eta = 0.656$ [49] and with different values of the confinement energy $\hbar\Omega_0$. In this case, the spin-polarized ground state changes to the ground state satisfying Hund’s rule with increasing $\hbar\Omega_0$ in the interval $0.0421H^* < \hbar\Omega_0 < 0.0422H^*$.

In the inset to Fig. 4, the first frequency moment of the optical conductivity

$$\langle \omega \rangle \equiv \frac{\int_0^\infty \omega \text{Re } \sigma(\omega) d\omega}{\int_0^\infty \text{Re } \sigma(\omega) d\omega}, \quad (45)$$

as a function of $\hbar\Omega_0$ shows a *discontinuity*, at the value of the confinement energy corresponding to the change of the shell filling schemes from the spin-polarized ground state to the ground state obeying Hund’s rule. This discontinuity should be observable in optical measurements.

In Fig. 5, the first frequency moment (45) is plotted as a function of the number of electrons for a CdSe quantum dot with $\Omega_0 = 0.143\omega_{\text{LO}}$ (corresponding to $\hbar\Omega_0 \approx 0.04 H^*$). The total spin of the system as a function of N is shown in the inset. As a general trend, $\langle \omega \rangle$ decreases with increasing N , with kinks corresponding to the ground-state transitions from states obeying Hund’s rule with $N = 3, 9$, and 18 , into spin-polarized states with $N = 4, 10$, and 19 , respectively.

In Fig. 6, optical conductivity spectra are plotted for several values of the confinement frequency for $N = 10$ polarons in a quantum dot with $\alpha = 2$, $\eta = 0.6$. These values of α and η are typical for the high- T_c superconducting cuprates of the NCCO family [29]. In the “weak-confinement” region ($\Omega_0 = 0.6\omega_{\text{LO}}$ and $\Omega_0 = 0.8\omega_{\text{LO}}$) the zero-phonon peak is expressively dominant over the other peaks.

When the confinement frequency parameter passes through the value $\Omega_0 = \omega_{\text{LO}}$, the so-called “confinement-phonon resonance” [38] occurs. In this case, the peaks at $\tilde{\Omega}_k, k = 1, 2, 3$ have comparable oscillator strengths. The position $\tilde{\Omega}_2$ of the second peak is substantially shifted from the LO phonon frequency ω_{LO} . Moreover, the intensities of the phonon-assisted transitions increase as compared to the “weak-confinement” case. This resonance has a clear analogy with the magneto-phonon resonance (see, e.g., Ref. [50]), as far as the energy levels of an electron in a parabolic confinement are similar to the Landau levels of an electron in a magnetic field.

With further increasing Ω_0 , when $\Omega_0 > \omega_{\text{LO}}$, the dominant part of the optical conductivity spectrum shifts to higher frequencies. For instance, at $\Omega_0 = 1.4\omega_{\text{LO}}$ the most intensive peak is that with $\tilde{\Omega}_3$. The intensities of the peaks, beginning with the second peak, increase in comparison with the intensities of their “weak-confinement” analogs. The positions of the zero-phonon line and the subsequent peaks are substantially shifted from the “weak-confinement” values towards higher frequencies. These effects are a manifestation of the

mixing of the zero-phonon state with different excited states of the many-polaron system. A similar behavior of the optical absorption spectra at and above the magneto-phonon resonance is explained by the mixing of zero-phonon and one-phonon quantum states [50].

The shell structure for a system of interacting polarons in a quantum dot is clearly revealed when analyzing the addition energy and the first frequency moment of the optical conductivity in parallel. In Figs. 7 and 8, we show both the function

$$\Theta(N) \equiv \langle \omega \rangle|_{N+1} - 2 \langle \omega \rangle|_N + \langle \omega \rangle|_{N-1}, \quad (46)$$

and the addition energy $\Delta(N)$ for interacting polarons in different 3D quantum dots.

As seen from Figs. 7 and 8 for quantum dots of CdSe and with $\alpha = 3$ [51], respectively, distinct peaks appear in $\Theta(N)$ and $\Delta(N)$ at the “magic numbers” corresponding to closed-shell configurations at $N = 8, 20$ for the states obeying Hund’s rule in panels *a, b* and to half-filled-shell configurations at $N = 10, 20$ for the spin-polarized states in panels *c, d* of Fig. 8. In the case when the shell filling scheme is the same for different N (see panels *a, b* in Figs. 7, 8, where the filling obeys Hund’s rule), each of the peaks of $\Theta(N)$ corresponds to a peak of the addition energy. In the case when the shell filling scheme changes with varying N (panels *c, d* in Figs. 7, 8), the function $\Theta(N)$ exhibits pronounced minima for N corresponding to the change of the filling scheme from the states, obeying Hund’s rule, to the spin-polarized states.

It follows that measurements of the addition energy and the first frequency moment of the optical absorption as a function of the number of polarons in a quantum dot can reflect the difference between open-shell and closed-shell configurations. In particular, the closed-shell configurations may be revealed through peaks in the function $\Theta(N)$. The filling patterns for a many-polaron system in a quantum dot can be determined from the analysis of the first moment of the optical absorption for different numbers of polarons. The appearance of minima in the function $\Theta(N)$ will then indicate a transition from the states which are filled according to Hund’s rule to the spin-polarized states.

VI. CONCLUSIONS

We presented a formalism for calculating the ground-state energy and the optical conductivity spectra of a system of N interacting polarons in a parabolic confinement potential for arbitrary electron-phonon coupling strength. The path integral treatment of the quantum statistics of indistinguishable particles [34, 36] allows us to find an upper bound [36] to the ground-state energy of a finite number of polarons. The parameters from the variational procedure are used as input for the calculation of the optical conductivity spectrum of the system.

Two types of transitions were found for N polarons confined in a parabolic potential, with the corresponding ground states characterized by different values of the total spin. In the weak-confinement regime, the polaron system is in the spin-polarized state. When increasing the confinement frequency Ω_0 , the system goes into a state obeying Hund’s rule at a specific value of Ω_0 . For a strongly coupled system of interacting polarons, a third type of state appears, for which the total spin takes its minimal value. The analysis is performed for both closed-shell and open-shell systems.

The calculations of the optical conductivity spectra for a finite number of polarons in a quantum dot are based on the memory-function approach. The dependence of the optical

conductivity spectra on the confinement parameter Ω_0 reveals a resonant behavior for $\Omega_0 \approx \omega_{\text{LO}}$. Transitions between states with different values of the total spin manifest themselves through discontinuous changes of the optical conductivity spectra and of the addition energy as a function of the number of electrons.

The first frequency moment of the optical conductivity as a function of the number of electrons clearly shows the transition between the spin-polarized ground state of interacting polarons in a quantum dot and the ground state obeying Hund's rule, and it also can be used to discriminate between open-shell and closed-shell configurations. Optical measurements are therefore suggested as possible tools for examining the shell structure of a system of interacting polarons.

Acknowledgments

Discussions with V. N. Gladilin are gratefully acknowledged. This work has been supported by the GOA BOF UA 2000, IUAP, FWO-V projects G.0306.00, G.0274.01N, G.0435.03, the WOG WO.025.99N (Belgium) and the European Commission GROWTH Programme, NANOMAT project, contract No. G5RD-CT-2001-00545.

This work is performed in the framework of the FWO-V projects Nos. G.0435.03, G.0306.00, the W.O.G. project WO.025.99N, and the GOA BOF UA 2000 project.

A. PARTITION FUNCTION OF THE MODEL SYSTEM

In this appendix we discuss the analytical calculation of the partition function $Z_0(\{N_\sigma\}, \beta)$ [Eq. (18)] for the model system of interacting polarons. It can be expressed in terms of the partition function $Z_M(\{N_\sigma\}, N_f, \beta)$ of the model system of interacting electrons and fictitious particles with the Lagrangian L_M [Eq. (17)] as follows:

$$Z_0(\{N_\sigma\}, \beta) = \frac{Z_M(\{N_\sigma\}, N_f, \beta)}{Z_f(N_f, w_f, \beta)}, \quad (\text{A.1})$$

where $Z_f(N_f, w_f, \beta)$ is the partition function of fictitious particles,

$$Z_f(N_f, \beta) = \frac{1}{(2 \sinh \frac{1}{2} \beta \hbar w_f)^{DN_f}}, \quad (\text{A.2})$$

with

$$w_f = \sqrt{\Omega_f^2 + kN/m_f} \quad (\text{A.3})$$

and $D=3(2)$ for 3D(2D) systems. The partition function $Z_M(\{N_\sigma\}, N_f, \beta)$ is the path integral for both the electrons and the fictitious particles:

$$Z_M(\{N_\sigma\}, N_f, \beta) = \sum_P \frac{(-1)^{\xi_P}}{N_{1/2}! N_{-1/2}!} \int d\bar{\mathbf{x}} \int_{\bar{\mathbf{x}}}^{P\bar{\mathbf{x}}} D\bar{\mathbf{x}}(\tau) \int d\bar{\mathbf{y}} \int_{\bar{\mathbf{y}}}^{\bar{\mathbf{y}}} D\bar{\mathbf{y}}(\tau) e^{-S_M[\bar{\mathbf{x}}(\tau), \bar{\mathbf{y}}(\tau)]} \quad (\text{A.4})$$

with the “action” functional

$$S_M [\bar{\mathbf{x}}(\tau), \bar{\mathbf{y}}(\tau)] = -\frac{1}{\hbar} \int_0^{\hbar\beta} L_M (\dot{\bar{\mathbf{x}}}, \dot{\bar{\mathbf{y}}}; \bar{\mathbf{x}}, \bar{\mathbf{y}}) d\tau, \quad (\text{A.5})$$

where the Lagrangian is given by Eq. (17).

Let us consider an auxiliary “ghost” subsystem with the Lagrangian

$$L_g (\dot{\mathbf{X}}_g, \dot{\mathbf{Y}}_g, \mathbf{X}_g, \mathbf{Y}_g) = -\frac{m_b N}{2} (\dot{\mathbf{X}}_g^2 + w^2 \mathbf{X}_g^2) - \frac{m_f N_f}{2} (\dot{\mathbf{Y}}_g^2 + w_f^2 \mathbf{Y}_g^2) \quad (\text{A.6})$$

with two frequencies w and w_f , where w is given by

$$w = \sqrt{\Omega^2 - N\omega^2 + kN_f/m_b}. \quad (\text{A.7})$$

The partition function Z_g of this subsystem

$$Z_g = \int d\mathbf{X}_g \int d\mathbf{Y}_g \int_{\mathbf{X}_g}^{\mathbf{X}_g} D\mathbf{X}_g(\tau) \int_{\mathbf{Y}_g}^{\mathbf{Y}_g} D\mathbf{Y}_g(\tau) \exp \{-S_g [\mathbf{X}_g(\tau), \mathbf{Y}_g(\tau)]\}, \quad (\text{A.8})$$

with the “action” functional

$$S_g [\mathbf{X}_g(\tau), \mathbf{Y}_g(\tau)] = -\frac{1}{\hbar} \int_0^{\hbar\beta} L_g (\dot{\mathbf{X}}_g, \mathbf{X}_g, \dot{\mathbf{Y}}_g, \mathbf{Y}_g) d\tau \quad (\text{A.9})$$

is readily calculated:

$$Z_g = \frac{1}{[2 \sinh(\frac{\beta\hbar w}{2})]^D} \frac{1}{[2 \sinh(\frac{\beta\hbar w_f}{2})]^D}. \quad (\text{A.10})$$

The product $Z_g Z_M$ of the two partition functions Z_g and $Z_M(\{N_\sigma\}, N_f, \beta)$ is a path integral in the state space of N electrons, N_f fictitious particles and two “ghost” particles with the coordinate vectors \mathbf{X}_g and \mathbf{Y}_g . The Lagrangian \tilde{L}_M of this system is a sum of L_M and L_g ,

$$\tilde{L}_M (\dot{\bar{\mathbf{x}}}, \dot{\bar{\mathbf{y}}}, \dot{\mathbf{X}}_g, \dot{\mathbf{Y}}_g; \bar{\mathbf{x}}, \bar{\mathbf{y}}, \mathbf{X}_g, \mathbf{Y}_g) \equiv L_M (\dot{\bar{\mathbf{x}}}, \dot{\bar{\mathbf{y}}}; \bar{\mathbf{x}}, \bar{\mathbf{y}}) + L_g (\dot{\mathbf{X}}_g, \dot{\mathbf{Y}}_g, \mathbf{X}_g, \mathbf{Y}_g). \quad (\text{A.11})$$

The “ghost” subsystem is introduced because the center-of-mass coordinates in \tilde{L}_M can be explicitly separated more easily than in L_M . This separation is realized by the linear transformation of coordinates,

$$\begin{cases} \mathbf{x}_{j,\sigma} = \mathbf{x}'_{j,\sigma} + \mathbf{X} - \mathbf{X}_g, \\ \mathbf{y}_{j\sigma} = \mathbf{y}'_{j\sigma} + \mathbf{Y} - \mathbf{Y}_g, \end{cases} \quad (\text{A.12})$$

where \mathbf{X} and \mathbf{Y} are the center-of-mass coordinate vectors of the electrons and of the fictitious particles, correspondingly:

$$\mathbf{X} = \frac{1}{N} \sum_{\sigma} \sum_{j=1}^{N_{\sigma}} \mathbf{x}_{j,\sigma}, \quad \mathbf{Y} = \frac{1}{N_f} \sum_{j=1}^{N_f} \mathbf{y}_j. \quad (\text{A.13})$$

Before the transformation (A.12), the independent variables are $(\bar{\mathbf{x}}, \bar{\mathbf{y}}, \mathbf{X}_g, \mathbf{Y}_g)$, with the center-of-mass coordinates \mathbf{X} and \mathbf{Y} determined by Eq. (A.13). After this transformation the independent variables can be considered to be $(\dot{\bar{\mathbf{x}}}', \dot{\bar{\mathbf{y}}}', \mathbf{X}, \mathbf{Y})$, where the coordinates $(\mathbf{X}_g, \mathbf{Y}_g)$ obey the equations

$$\mathbf{X}_g = \frac{1}{N} \sum_{\sigma} \sum_{j=1}^{N_{\sigma}} \mathbf{x}'_{j,\sigma}, \quad \mathbf{Y}_g = \frac{1}{N_f} \sum_{j=1}^{N_f} \mathbf{y}'_j. \quad (\text{A.14})$$

A substitution of Eq. (A.13) into Eq. (A.11) results in the following 3 terms:

$$\tilde{L}_M \left(\dot{\bar{\mathbf{x}}}', \dot{\bar{\mathbf{y}}}', \dot{\mathbf{X}}, \dot{\mathbf{Y}}; \bar{\mathbf{x}}', \bar{\mathbf{y}}', \mathbf{X}, \mathbf{Y} \right) = L_w \left(\dot{\bar{\mathbf{x}}}', \bar{\mathbf{x}}' \right) + L_{w_f} \left(\dot{\bar{\mathbf{y}}}', \bar{\mathbf{y}}' \right) + L_C \left(\dot{\mathbf{X}}, \mathbf{X}; \dot{\mathbf{Y}}, \mathbf{Y} \right), \quad (\text{A.15})$$

where $L_w \left(\dot{\bar{\mathbf{x}}}', \bar{\mathbf{x}}' \right)$ and $L_{w_f} \left(\dot{\bar{\mathbf{y}}}', \bar{\mathbf{y}}' \right)$ are Lagrangians of non-interacting identical oscillators with the frequencies w and w_f , respectively,

$$L_w \left(\dot{\bar{\mathbf{x}}}', \bar{\mathbf{x}}' \right) = -\frac{m_b}{2} \sum_{\sigma=\pm 1/2} \sum_{j=1}^{N_{\sigma}} \left[(\dot{\mathbf{x}}'_{j,\sigma})^2 + w^2 (\mathbf{x}'_{j,\sigma})^2 \right], \quad (\text{A.16})$$

$$L_{w_f} \left(\dot{\bar{\mathbf{y}}}', \bar{\mathbf{y}}' \right) = -\frac{m_f}{2} \sum_{j=1}^{N_f} \left[(\dot{\mathbf{y}}'_{j,\sigma})^2 + w_f^2 (\mathbf{y}'_{j,\sigma})^2 \right]. \quad (\text{A.17})$$

The Lagrangian $L_C \left(\dot{\mathbf{X}}, \mathbf{X}; \dot{\mathbf{Y}}, \mathbf{Y} \right)$ describes the combined motion of the centers-of-mass of the electrons and of the fictitious particles,

$$L_C \left(\dot{\mathbf{X}}, \mathbf{X}; \dot{\mathbf{Y}}, \mathbf{Y} \right) = -\frac{m_b N}{2} \left(\dot{\mathbf{X}}^2 + \tilde{\Omega}^2 \mathbf{X}^2 \right) - \frac{m_f N_f}{2} \left(\dot{\mathbf{Y}}^2 + w_f^2 \mathbf{Y}^2 \right) + k N N_f \mathbf{X} \cdot \mathbf{Y}, \quad (\text{A.18})$$

with

$$\tilde{\Omega} = \sqrt{\Omega^2 + k N_f / m_b}. \quad (\text{A.19})$$

It is reduced to a diagonal quadratic form in the coordinates and the velocities by a standard transformation for two interacting oscillators:

$$\begin{aligned} \mathbf{X} &= \frac{1}{\sqrt{m_b N}} (a_1 \mathbf{r} + a_2 \mathbf{R}), \\ \mathbf{Y} &= \frac{1}{\sqrt{m_f N_f}} (-a_2 \mathbf{r} + a_1 \mathbf{R}) \end{aligned} \quad (\text{A.20})$$

with the coefficients

$$a_1 = \left[\frac{1 + \chi}{2} \right]^{1/2}, \quad a_2 = \left[\frac{1 - \chi}{2} \right]^{1/2}, \quad (\text{A.21})$$

$$\chi \equiv \frac{\tilde{\Omega}^2 - \tilde{\Omega}_f^2}{\left[\left(\tilde{\Omega}^2 - \tilde{\Omega}_f^2 \right)^2 + 4\gamma^2 \right]^{1/2}}, \quad \gamma \equiv k \sqrt{\frac{N N_f}{m_b m_f}}. \quad (\text{A.22})$$

The eigenfrequencies of the center-of-mass subsystem are then given by the expression

$$\begin{cases} \Omega_1 = \sqrt{\frac{1}{2} \left[\tilde{\Omega}^2 + \tilde{\Omega}_f^2 + \sqrt{\left(\tilde{\Omega}^2 - \tilde{\Omega}_f^2 \right)^2 + 4\gamma^2} \right]}, \\ \Omega_2 = \sqrt{\frac{1}{2} \left[\tilde{\Omega}^2 + \tilde{\Omega}_f^2 - \sqrt{\left(\tilde{\Omega}^2 - \tilde{\Omega}_f^2 \right)^2 + 4\gamma^2} \right]}. \end{cases} \quad (\text{A.23})$$

As a result, four independent frequencies Ω_1 , Ω_2 , w and w_f appear in the problem. Three of them (Ω_1 , Ω_2 , w) are the eigenfrequencies of the model system. Ω_1 is the frequency of the relative motion of the center of mass of the electrons with respect to the center of mass of the fictitious particles; Ω_2 is the frequency related to the center of mass of the model system as a whole; w is the frequency of the relative motion of the electrons with respect to their center of mass. The parameter w_f is an analog of the second variational parameter w of the one-polaron Feynman model. Further, the Lagrangian (A.18) takes the form

$$L_C = -\frac{1}{2} (\dot{\mathbf{r}}^2 + \Omega_1^2 \mathbf{r}^2) - \frac{1}{2} (\dot{\mathbf{R}}^2 + \Omega_2^2 \mathbf{R}^2), \quad (\text{A.24})$$

leading to the partition function corresponding to the combined motion of the centers-of-mass of the electrons and of the fictitious particles

$$Z_C = \frac{1}{[2 \sinh(\frac{\beta \hbar \Omega_1}{2})]^D} \frac{1}{[2 \sinh(\frac{\beta \hbar \Omega_2}{2})]^D}. \quad (\text{A.25})$$

Taking into account Eqs. (A.10) and (A.25), we obtain finally the partition function of the model system for interacting polarons

$$Z_0(\{N_\sigma\}, \beta) = \left[\frac{\sinh(\frac{\beta \hbar w}{2}) \sinh(\frac{\beta \hbar w_f}{2})}{\sinh(\frac{\beta \hbar \Omega_1}{2}) \sinh(\frac{\beta \hbar \Omega_2}{2})} \right]^D \tilde{Z}_F(\{N_\sigma\}, w, \beta). \quad (\text{A.26})$$

Here

$$\tilde{Z}_F(\{N_\sigma\}, w, \beta) = \mathbb{Z}_F(N_{1/2}, w, \beta) \mathbb{Z}_F(N_{-1/2}, w, \beta) \quad (\text{A.27})$$

is the partition function of $N = N_{1/2} + N_{-1/2}$ non-interacting fermions in a parabolic confinement potential with the frequency w . The analytical expressions for the partition function of N_σ spin-polarized fermions $\mathbb{Z}_F(N_\sigma, w, \beta)$ were derived in Ref. [34].

B. TWO-POINT CORRELATION FUNCTION. MEMORY FUNCTION.

The two-point correlation function (22) is represented as the following path integral:

$$g(\mathbf{q}, \tau | \{N_\sigma\}, \beta) = \frac{1}{Z_0(\{N_\sigma\}, \beta)} \sum_P \frac{(-1)^{\xi_P}}{N_{1/2}! N_{-1/2}!} \int d\bar{\mathbf{x}} \int_{\bar{\mathbf{x}}}^{P\bar{\mathbf{x}}} D\bar{\mathbf{x}}(\tau) e^{-S_0[\bar{\mathbf{x}}(\tau)]} \rho_{\mathbf{q}}(\tau) \rho_{-\mathbf{q}}(0). \quad (\text{B.1})$$

We observe that $g(\mathbf{q}, \tau | \{N_\sigma\}, \beta)$ can be rewritten as an average within the model “action” $S_M[\bar{\mathbf{x}}(\tau), \bar{\mathbf{y}}(\tau)]$ of interacting electrons and fictitious particles:

$$\begin{aligned} g(\mathbf{q}, \tau | \{N_\sigma\}, \beta) &= \frac{1}{Z_M(\{N_\sigma\}, N_f, \beta)} \sum_P \frac{(-1)^{\xi_P}}{N_{1/2}! N_{-1/2}!} \\ &\times \int d\bar{\mathbf{x}} \int_{\bar{\mathbf{x}}}^{P\bar{\mathbf{x}}} D\bar{\mathbf{x}}(\tau) \int d\bar{\mathbf{y}} \int_{\bar{\mathbf{y}}}^{\bar{\mathbf{y}}} D\bar{\mathbf{y}}(\tau) e^{-S_M[\bar{\mathbf{x}}(\tau), \bar{\mathbf{y}}(\tau)]} \\ &\times \rho_{\mathbf{q}}(\tau) \rho_{-\mathbf{q}}(0). \end{aligned} \quad (\text{B.2})$$

Indeed, one readily derives that the elimination of the fictitious particles in (B.2) leads to (B.1). The representation (B.2) allows one to calculate the correlation function $g(\mathbf{q}, \tau | \{N_\sigma\}, \beta)$ in a much simpler way than through Eq. (B.1), using the separation of the coordinates of the centers of mass of the electrons and of the fictitious particles. This separation is performed for the two-point correlation function (B.2) by the same method as it has been done for the partition function (A.4). As a result, one obtains

$$g(\mathbf{q}, \tau | \{N_\sigma\}, \beta) = \tilde{g}(\mathbf{q}, \tau | \{N_\sigma\}, \beta) \frac{\langle \exp[i\mathbf{q} \cdot (\mathbf{X}(\tau) - \mathbf{X}(\sigma))] \rangle_{S_C}}{\langle \exp[i\mathbf{q} \cdot (\mathbf{X}_g(\tau) - \mathbf{X}_g(\sigma))] \rangle_{S_g}}, \quad (\text{B.3})$$

where $\tilde{g}(\mathbf{q}, \tau | \{N_\sigma\}, \beta)$ is the time-dependent correlation function of N non-interacting electrons in a parabolic confinement potential with the frequency w ,

$$\tilde{g}(\mathbf{q}, \tau | \{N_\sigma\}, \beta) = \langle \rho_{\mathbf{q}}(\tau) \rho_{-\mathbf{q}}(0) \rangle_{S_w}. \quad (\text{B.4})$$

The action functional $S_w[\bar{\mathbf{x}}_\tau]$ is related to the Lagrangian $L_w(\dot{\bar{\mathbf{x}}}, \bar{\mathbf{x}})$ [Eq. (A.16)]

$$S_w[\bar{\mathbf{x}}_\tau] = \frac{1}{\hbar} \int_0^{\hbar\beta} L_w(\dot{\bar{\mathbf{x}}}, \bar{\mathbf{x}}) d\tau. \quad (\text{B.5})$$

The averages in (B.3) are calculated using Feynman’s method of generating functions [39],

$$\begin{aligned} \langle \exp[i\mathbf{q} \cdot (\mathbf{X}(\tau) - \mathbf{X}(\sigma))] \rangle_{S_C} &= \exp \left\{ -\frac{\hbar q^2}{Nm_b} \left[\sum_{i=1}^2 a_i^2 \frac{\sinh\left(\frac{\Omega_i|\tau-\sigma|}{2}\right) \sinh\left(\frac{\Omega_i(\hbar\beta-|\tau-\sigma|)}{2}\right)}{\Omega_i \sinh\left(\frac{\beta\hbar\Omega_i}{2}\right)} \right] \right\}, \\ \langle \exp[i\mathbf{q} \cdot (\mathbf{X}_g(\tau) - \mathbf{X}_g(\sigma))] \rangle_{S_g} &= \exp \left[-\frac{\hbar q^2}{Nm_b} \frac{\sinh\left(\frac{w|\tau-\sigma|}{2}\right) \sinh\left(\frac{w(\hbar\beta-|\tau-\sigma|)}{2}\right)}{w \sinh\left(\frac{\beta\hbar w}{2}\right)} \right]. \end{aligned}$$

The two-point correlation function $\tilde{g}(\mathbf{q}, \tau | \{N_\sigma\}, \beta)$ is derived using the generating-function technique for identical particles [34]. After the path integration, the following expression is obtained:

$$\begin{aligned} &\tilde{g}(\mathbf{q}, -i\tau | \{N_\sigma\}, \beta) \\ &= \sum_{\mathbf{n}, \sigma, \mathbf{n}', \sigma'} (e^{i\mathbf{q} \cdot \mathbf{x}})_{\mathbf{nn}} (e^{-i\mathbf{q} \cdot \mathbf{x}})_{\mathbf{n}'\mathbf{n}'} f_2(n, \sigma; n', \sigma' | \{N_\sigma\}, \beta) \\ &+ \sum_{\mathbf{n}, \mathbf{n}', \sigma} |(e^{i\mathbf{q} \cdot \mathbf{x}})_{\mathbf{nn}'}|^2 \exp \left[\frac{\tau}{\hbar} (\varepsilon_n - \varepsilon_{n'}) \right] \\ &\times [f_1(n, \sigma | \{N_\sigma\}, \beta) - f_2(n, \sigma; n', \sigma' | \{N_\sigma\}, \beta)], \end{aligned} \quad (\text{B.6})$$

where $(e^{i\mathbf{q}\cdot\mathbf{x}})_{\mathbf{nn}'}$ is the one-electron matrix element,

$$(e^{i\mathbf{q}\cdot\mathbf{x}})_{\mathbf{nn}'} = \int e^{i\mathbf{q}\cdot\mathbf{x}} \psi_{\mathbf{n}}^*(\mathbf{x}) \psi_{\mathbf{n}'}(\mathbf{x}) d\mathbf{x}. \quad (\text{B.7})$$

For a 3D quantum dot, $\psi_{\mathbf{n}}(\mathbf{x})$ is the eigenfunction of a 3D oscillator with the frequency w [see, e.g., Ref. [52]]. The index \mathbf{n} denotes the set $\mathbf{n} = (n, l, m)$, where n is the number of the energy level $\varepsilon_n = \hbar w (n + 3/2)$, l is the quantum number of the orbital angular momentum and m is the quantum number of the z projection of the orbital angular momentum. Similarly, for a 2D quantum dot, $\psi_{\mathbf{n}}(\mathbf{x})$ is the eigenfunction of a 2D oscillator with the frequency w .

The one-electron distribution function $f_1(n, \sigma | N_\sigma, \beta)$ is the average number of electrons with the spin projection σ at the n -th energy level, while the two-electron distribution function $f_2(n, \sigma; n', \sigma' | \{N_\sigma\}, \beta)$ is the average product of the numbers of electrons with the spin projections σ and σ' at the levels n and n' . These functions are expressed through the following integrals (cf. Ref. [35]):

$$f_1(n, \sigma | N_\sigma, \beta) = \frac{1}{2\pi \mathbb{Z}_F(N_\sigma, w, \beta)} \int_{-\pi}^{\pi} f(\varepsilon_n, \theta) \Phi(\theta, \beta, N_\sigma) d\theta, \quad (\text{B.8})$$

$$f_2(n, \sigma; n', \sigma' | \{N_\sigma\}, \beta) = \begin{cases} \frac{1}{2\pi \mathbb{Z}_F(N_\sigma, w, \beta)} \int_{-\pi}^{\pi} f(\varepsilon_n, \theta) f(\varepsilon_{n'}, \theta) \Phi(\theta, \beta, N_\sigma) d\theta, & \text{if } \sigma' = \sigma; \\ f_1(n, \sigma | N_\sigma, \beta) f_1(n', \sigma' | N_{\sigma'}, \beta), & \text{if } \sigma' \neq \sigma \end{cases} \quad (\text{B.9})$$

with the notations

$$\Phi(\theta, \beta, N_\sigma) = \exp \left[\sum_{n=0}^{\infty} \ln(1 + e^{i\theta + \xi - \beta \varepsilon_n}) - N_\sigma(\xi + i\theta) \right], \quad (\text{B.10})$$

$$f(\varepsilon, \theta) \equiv \frac{1}{\exp(\beta \varepsilon - \xi - i\theta) + 1}. \quad (\text{B.11})$$

The function $f(\varepsilon, \theta)$ formally coincides with the Fermi-Dirac distribution function of the energy ε with the “chemical potential” $(\xi + i\theta)/\beta$.

From here on we consider the zero-temperature limit, for which the integrals (B.8) and (B.9) can be calculated analytically. The result for the one-electron distribution function is

$$f_1(n, \sigma | \beta, N_\sigma) |_{\beta \rightarrow \infty} = \begin{cases} 1, & n < L_\sigma; \\ 0, & n > L_\sigma; \\ \frac{N_\sigma - N_{L_\sigma}}{g_{L_\sigma}}, & n = L_\sigma. \end{cases} \quad (\text{B.12})$$

According to (B.12), L_σ is the number of the lowest open shell, and

$$g_n = \begin{cases} \frac{1}{2}(n+1)(n+2) & (3D), \\ n+1 & (2D). \end{cases}$$

is the degeneracy of the n -th shell. N_{L_σ} is the number of electrons in all the closed shells with the spin projection σ ,

$$N_{L_\sigma} \equiv \sum_{n=0}^{L_\sigma-1} g_n = \begin{cases} \frac{1}{6} L_\sigma (L_\sigma + 1) (L_\sigma + 2) & (3D), \\ \frac{1}{2} L_\sigma (L_\sigma + 1) & (2D). \end{cases} \quad (\text{B.13})$$

The two-electron distribution function $f_2(n, \sigma; n', \sigma' | \{N_\sigma\}, \beta)$ at $T = 0$ takes the form

$$f_2(n, \sigma; n', \sigma' | \beta, \{N_\sigma\})|_{\beta \rightarrow \infty} = \begin{cases} f_1(n, \sigma | \beta, N_\sigma)|_{\beta \rightarrow \infty} f_1(n', \sigma' | \beta, N_{\sigma'})|_{\beta \rightarrow \infty}, & n \neq n' \text{ or } \sigma \neq \sigma' \\ 1, & \sigma = \sigma' \text{ and } n = n' < L_\sigma; \\ 0, & \sigma = \sigma' \text{ and } n = n' > L_\sigma; \\ \frac{N - N_{L_\sigma}}{g_{L_\sigma}} \frac{N - N_{L_\sigma} - 1}{g_{L_\sigma} - 1}, & \sigma = \sigma' \text{ and } n = n' = L_\sigma. \end{cases} \quad (\text{B.14})$$

Finally, using the two-point correlation function Eq. (B.7), the one-electron (B.12) and the two-electron (B.14) distribution functions, the memory function of Eq. (42) can be represented in the unified form for 3D and 2D interacting polarons:

$$\begin{aligned} \chi(\omega) = & \lim_{\varepsilon \rightarrow +0} \frac{2\alpha}{3\pi N} \left(\frac{3\pi}{4}\right)^{3-D} \left(\frac{\omega_{\text{LO}}}{A}\right)^{3/2} \\ & \times \sum_{p_1=0}^{\infty} \sum_{p_2=0}^{\infty} \sum_{p_3=0}^{\infty} \frac{(-1)^{p_3}}{p_1! p_2! p_3!} \left(\frac{a_1^2}{N\Omega_1 A}\right)^{p_1} \left(\frac{a_2^2}{N\Omega_2 A}\right)^{p_2} \left(\frac{1}{NwA}\right)^{p_3} \\ & \times \left\{ \left[\sum_{m=0}^{\infty} \sum_{n=0}^{\infty} \sum_{\sigma} [f_1(n, \sigma | \{N_\sigma\}, \beta) - f_2(n, \sigma; m, \sigma' | \{N_\sigma\}, \beta)]|_{\beta \rightarrow \infty} \right. \right. \\ & \times \left(\frac{1}{\omega - \omega_{\text{LO}} - [p_1\Omega_1 + p_2\Omega_2 + (p_3 - m + n)w] + i\varepsilon} - \frac{1}{\omega + \omega_{\text{LO}} + p_1\Omega_1 + p_2\Omega_2 + (p_3 - m + n)w + i\varepsilon} \right) \\ & \left. + \mathcal{P} \left(\frac{2}{\omega_{\text{LO}} + p_1\Omega_1 + p_2\Omega_2 + (p_3 - m + n)w} \right) \right] \\ & \times \sum_{l=0}^m \sum_{k=n-m+l}^n \frac{(-1)^{n-m+l+k} \Gamma(p_1 + p_2 + p_3 + k + l + \frac{3}{2})}{k! l!} \left(\frac{1}{wA}\right)^{l+k} \\ & \times \binom{n+D-1}{n-k} \binom{2k}{k-l-n+m} \Bigg] \\ & + \left[\left(\frac{1}{\omega - \omega_{\text{LO}} - (p_1\Omega_1 + p_2\Omega_2 + p_3w) + i\varepsilon} - \frac{1}{\omega + \omega_{\text{LO}} + p_1\Omega_1 + p_2\Omega_2 + p_3w + i\varepsilon} \right) \right. \\ & \left. + \mathcal{P} \left(\frac{2}{\omega_{\text{LO}} + p_1\Omega_1 + p_2\Omega_2 + p_3w} \right) \right] \\ & \times \sum_{m=0}^{\infty} \sum_{n=0}^{\infty} \sum_{\sigma, \sigma'} f_2(n, \sigma; m, \sigma' | \{N_\sigma\}, \beta)|_{\beta \rightarrow \infty} \\ & \times \sum_{k=0}^n \sum_{l=0}^m \frac{(-1)^{k+l} \Gamma(p_1 + p_2 + p_3 + k + l + \frac{3}{2})}{k! l!} \left(\frac{1}{wA}\right)^{k+l} \\ & \times \left. \binom{n+D-1}{n-k} \binom{m+D-1}{m-l} \right] \Bigg\}, \end{aligned} \quad (\text{B.15})$$

where $D = 2, 3$ is the dimensionality of the space, \mathcal{P} denotes the principal value, A is defined as $A \equiv [\sum_{i=1}^2 a_i^2 / \Omega_i + (N - 1) / w] / N$, Ω_1, Ω_2 , and w are the eigenfrequencies of the model system, a_1 and a_2 are the coefficients of the canonical transformation which diagonalizes the model Lagrangian (17) derived in Appendix A.

The typical spectra of the real and imaginary parts of the memory function $\chi(\omega)$, are plotted in Figs. 9(a) and 9(b), respectively. According to Eq. (B.15), the poles of $\text{Re } \chi(\omega)$ and the δ -like peaks of $[-\text{Im } \chi(\omega)]$ are positioned at the combinatorial frequencies ω_{klm} ,

which are linear combinations of the LO-phonon frequency and three eigenfrequencies

$$\omega_{klm} \equiv \omega_{\text{LO}} + k\Omega_1 + l\Omega_2 + mw, \quad (\text{B.16})$$

with integer coefficients $k, l, m = 0, 1, \dots$. Each combinatorial frequency ω_{klm} corresponds to a phonon-assisted transition to an excited state of the model system.

The roots of the equation (44), which provide the peaks in the optical conductivity, $(\tilde{\Omega}_1, \tilde{\Omega}_2, \dots)$, are indicated in Fig. 9a by the vertical arrows. For the chosen parameters, the peak at $\tilde{\Omega}_1$ is the zero-phonon line. Fig. 9a also reveals peaks of $\text{Re } \sigma(\omega)$ with frequencies in between two neighboring discrete values of ω_{nkl} , e.g., at $\tilde{\Omega}_2$. Following the physical interpretation of the memory function in Refs. [25, 26, 53], these peaks can be related to transitions into excited states of the many-polaron system.

-
- [*] Permanent address: Department of Theoretical Physics, State University of Moldova, str. A. Mateevici 60, MD-2009 Kishinev, Republic of Moldova.
 - [**] Also at Technische Universiteit Eindhoven, P. B. 513, 5600 MB Eindhoven, The Netherlands.
 - [1] C. Yannouleas and U. Landman, Phys. Rev. Lett. **82**, 5325 (1999).
 - [2] B. Bednarek, B. Szafran, and J. Adamowski, Phys. Rev. B **59**, 13036 (1999).
 - [3] B. Szafran, J. Adamowski, and S. Bednarek, Phys. Rev. B **61**, 1971 (2000).
 - [4] I.-H. Lee, V. Rao, R. M. Martin, and J.-P. Leburton, Phys. Rev. B **57**, 9035 (1998).
 - [5] K. Hirose, and N. S. Wingreen, Phys. Rev. B **59**, 4604 (1999).
 - [6] S. M. Reimann, M. Koskinen, J. Kolehmainen, M. Manninen, D. G. Austing, and S. Tarucha, Eur. Phys. J. D **9**, 105 (1999).
 - [7] Y.-H. Kim, I.-H. Lee, S. Nagaraja, J.-P. Leburton, R. Q. Hood, and R. M. Martin, Phys. Rev. B **61**, 5202 (2000).
 - [8] T. F. Jiang, X.-M. Tong, and S.-I. Chu, Phys. Rev. B **63**, 045317 (2001).
 - [9] B. Partoens and F. M. Peeters, Physica E **6**, 577 (2000).
 - [10] B. Partoens and F. M. Peeters, Phys. Rev. Lett. **84**, 4433 (2000).
 - [11] R. Egger, W. Häusler, C. H. Mak, and H. Grabert, Phys. Rev. Lett. **82**, 3320 (1999).
 - [12] A. Gonzalez, B. Partoens, and F. M. Peeters, Phys. Rev. B **56**, 15740 (1997).
 - [13] A. Gonzalez, B. Partoens, A. Matulis, and F. M. Peeters, Phys. Rev. B **59**, 1653 (1999).
 - [14] S. M. Reimann, M. Koskinen, and M. Manninen, Phys. Rev. B **62**, 8108 (2000).
 - [15] V.M. Fomin, V.N. Gladilin, J.T. Devreese, E.P. Pokatilov, S.N. Balaban, and S.N. Klimin, Phys. Rev. B **57**, 2415 (1998).
 - [16] L. Genzel, A. Wittlin, M. Bayer, M. Cardona, E. Schonherr, and A. Simon, Phys. Rev. B **40**, 2170 (1989).
 - [17] G. A. Thomas, D. H. Rapkine, S.-W. Cheong, and L. F. Schneemeyer, Phys. Rev. B **47**, 11369 (1993).
 - [18] P. Calvani, M. Capizzi, S. Lupi, P. Maselli, A. Paolone, P. Roy, S.-W. Cheong, W. Sadowski, and E. Walker, Solid State Communications **91**, 113 (1994).
 - [19] P. Calvani, M. Capizzi, S. Lupi, P. Maselli, and A. Paolone, Phys. Rev. B **53**, 2756 (1996).
 - [20] S. Lupi, M. Capizzi, P. Calvani, B. Ruzicka, P. Maselli, P. Dore, and A. Paolone, Phys. Rev. B **57**, 1248 (1998).
 - [21] J. T. Devreese and J. Tempere, Solid State Commun. **106**, 309 (1998).

- [22] S. Lupi, P. Maselli, M. Capizzi, P. Calvani, P. Giura, and P. Roy, Phys. Rev. Lett. **83**, 4852 (1999).
- [23] D. Emin, Phys. Rev. B **48**, 13691 (1993).
- [24] Eagles, D. M., Lobo, R. P. S. M., and Gervais, F., *Phys. Rev. B* **52**, 6440 - 6450 (1995).
- [25] J. Devreese, J. De Sitter, and M. Goovaerts, Phys. Rev. B **5**, 2367 (1972).
- [26] J. T. Devreese, in: *Polarons in Ionic Crystals and Polar Semiconductors* (North-Holland, Amsterdam, 1972), pp. 83 – 159.
- [27] J.T. Devreese, “Polarons”, in: *Encyclopedia of Applied Physics*, Vol. 14, pp. 383–413 (VHC Publishers, Weinheim, 1996).
- [28] R. P. Feynman, Phys. Rev. **97**, 660 (1955).
- [29] J. Tempere and J. T. Devreese, Phys. Rev. B **64**, 104504 (2001).
- [30] J. Tempere and J. T. Devreese, Eur. Phys. J. B **20**, 27 (2001).
- [31] L. F. Lemmens, J. T. Devreese, and F. Brosens, Phys. Stat. Sol. (b) **82**, 439 (1977).
- [32] V. Cataudella, G. De Filippis, and G. Iadonisi, European Physical Journal B **12**, 17 (1999).
- [33] J. T. Devreese, “Polarons” in: *Lectures on the Physics of Highly Correlated Electron Systems VII*, Eds. A. Avella, F. Mancini (AIP, Melville, 2003), pp. 3-56.
- [34] F. Brosens, J. T. Devreese, and L. F. Lemmens, Phys. Rev. E **55**, 227 (1997); **55**, 6795 (1997); **58**, 1634 (1998).
- [35] L. F. Lemmens, F. Brosens, and J. T. Devreese, Solid State Commun. **109**, 615 (1999).
- [36] L. F. Lemmens, F. Brosens, and J. T. Devreese, Phys. Rev. E **53**, 4467 (1996).
- [37] J. T. Devreese, in: *Fluctuating Paths and Fields* (World Scientific, Singapore, 2001), pp. 289-304.
- [38] J. T. Devreese, S. N. Klimin, V. M. Fomin, and F. Brosens, Solid State Communications **114**, 305 (2000).
- [39] R. P. Feynman, *Statistical Mechanics* (Benjamin, Massachusetts, 1972).
- [40] A. Messiah, Quantum Mechanics (North-Holland, Amsterdam, 1966), vol. 2, p. 702.
- [41] F. Rapisarda and G. Senatore, Aust. J. Phys. **49**, 161 (1996).
- [42] X. M. Tong and S. I. Chu, Phys. Rev. A **55**, 3406 (1997).
- [43] S. Tarucha, D. G. Austing, T. Honda, R. J. van der Hage, and L. P. Kouwenhoven, Phys. Rev. Letters **77**, 3613 (1996).
- [44] Xiaoguang Wu, F. M. Peeters, and J. T. Devreese, Phys. Rev. B **34**, 2621 (1986).
- [45] K. K. Thornber and R. P. Feynman, Phys. Rev. B **1**, 4099 (1970).
- [46] J. T. Devreese and V. M. Fomin, Phys. Rev. B **54**, 3959 (1996).
- [47] R. P. Feynman and A. R. Hibbs, *Quantum mechanics and path integrals*, McGraw-Hill, New York, 1965.
- [48] J. T. Devreese, L. F. Lemmens, and J. Van Royen, Phys. Rev. B **15**, 1212 (1977).
- [49] E. Kartheuser, in: *Polarons in Ionic Crystals and Polar Semiconductors* (North-Holland, Amsterdam, 1972), pp. 717-733.
- [50] D.J. Barnes, R.J. Nicholas, F.M. Peeters, X.-G. Wu, J.T. Devreese, J. Singleton, C.J.G.M. Langerak, J.J. Harris, C.T. Foxon, Phys. Rev. Lett. **66**, 794 (1991).
- [51] Future technological progress might allow one to fabricate quantum dots of materials with relatively large values of α .
- [52] C. Cohen-Tannoudji, B. Diu, and F. Laoë, *Quantum Mechanics* (John Wiley & Sons, New York; Hermann, Paris, 1977).
- [53] J. T. Devreese, S. N. Klimin, and V. M. Fomin, Phys. Rev. B **63**, 184307 (2001).
- [54] S. I. Pekar, *Research on Electron Theory in Crystals* (Gostekhizdat, Moscow and

- Leningrad, 1951) [in Russian; English translation: US AEC, Washington DC, 1963].
- [55] S. J. Miyake, J. Phys. Soc. Japan **41**, 747 (1976).
 - [56] J. Adamowski, Phys. Rev. B **39**, 3649 (1989).
 - [57] A. S. Mishchenko, N. V. Prokof'ev, A. Sakamoto, and B. V. Svistunov, Phys. Rev. B **62**, 6317 (2000).
 - [58] G. De Filippis, V. Cataudella, V. M. Ramaglia, C. A. Perroni, and D. Bercioux, Eur. Phys. Journal B **36**, 65 (2003).
 - [59] G. Verbist, F. M. Peeters, and J. T. Devreese, Phys. Rev. B **43**, 2712 (1991).
 - [60] E. P. Pokatilov, V. M. Fomin, J. T. Devreese, S. N. Balaban, and S. N. Klimin, Phys. Rev. B **61**, 2721 (2000).
 - [61] E. P. Pokatilov, M. D. Croitoru, V. M. Fomin, and J. T. Devreese, Phys. Stat. Sol. (b) **237**, 244 (2003).

Figure captions

Fig. 1. Total spin of a system of interacting polarons in a parabolic quantum dot as a function of the number of electrons for $\hbar\Omega_0 = 0.5H^*(a)$ and for $\hbar\Omega_0 = 0.1H^*(b)$.

Fig. 2. Addition energy of a system of interacting polarons in a parabolic quantum dot as a function of the number of electrons for $\hbar\Omega_0 = 0.5H^*(a)$ and for $\hbar\Omega_0 = 0.1H^*(b)$.

Fig. 3. The total spin (*a*) and the addition energy (*b*) of a system of interacting polarons in a 2D parabolic GaAs quantum dot as a function of the number of electrons for $\hbar\Omega_0 = 0.5H^*$. Inset: the experimentally observed addition energy vs number of electrons in a cylindrical GaAs quantum dot for two values of the diameter $D = 0.5\mu\text{m}$ and $D = 0.44\mu\text{m}$ [43].

Fig. 4. Optical conductivity spectra of $N = 20$ interacting polarons in CdSe quantum dots with $\alpha = 0.46$, $\eta = 0.656$ for different confinement energies close to the transition from a spin-polarized ground state to a ground state obeying Hund's rule. *Inset*: the first frequency moment $\langle\omega\rangle$ of the optical conductivity as a function of the confinement energy.

Fig. 5. The first frequency moment $\langle\omega\rangle$ of the optical conductivity as a function of the number of electrons for systems of interacting polarons in CdSe quantum dots with $\alpha = 0.46$, $\eta = 0.656$ and $0.143\omega_{\text{LO}}$ ($\hbar\Omega_0 \approx 0.04H^*$). Open squares denote the spin-polarized ground state; full dots denote the ground state, obeying Hund's rule; open triangles denote the ground state of the third type, with more than one partly filled shells, which is not totally spin-polarized. *Inset*: the total spin of the system of interacting polarons as a function of N .

Fig. 6. Optical conductivity spectra of $N = 10$ interacting polarons in a quantum dot with $\alpha = 2$, $\eta = 0.6$ for several values of the confinement frequency from $\Omega_0 = 0.6\omega_{\text{LO}}$ to $\Omega_0 = 1.4\omega_{\text{LO}}$. The spectrum for $\Omega_0 = \omega_{\text{LO}}$ corresponds to the confinement-phonon resonance.

Fig. 7. The function $\Theta(N)$ and the addition energy $\Delta(N)$ for systems of interacting polarons in CdSe quantum dots with $\alpha = 0.46$, $\eta = 0.656$ for $\hbar\Omega_0 = 0.1H^*$ (panels *a, b*) and for $\Omega_0 = 0.04H^*$ (panels *c, d*). Open squares denote the spin-polarized ground state; full dots denote the ground state, obeying Hund's rule; open triangles denote the ground state of the third type, with more than one partly filled shells, which is not totally spin-polarized.

Fig. 8. The function $\Theta(N)$ and the addition energy $\Delta(N)$ for systems of interacting polarons in quantum dots with $\alpha = 3$, $\eta = 0.25$ and $\Omega_0 = \omega_{\text{LO}}$ (panels *a, b*) and with $\alpha = 3$, $\eta = 0.3$ and $\Omega_0 = 0.5\omega_{\text{LO}}$ (panels *c, d*).

Fig. 9. Real (*a*) and imaginary (*b*) parts of the memory function $\chi(\omega)/\omega$ for a system of interacting polarons in a quantum dot for $N = 10$, $\alpha = 2$, $\eta = 0.6$, and $\Omega_0 = 0.6\omega_{\text{LO}}$. The dashed line in panel *a* represents $(\omega^2 - \Omega_0^2)/\omega$. The vertical arrows in panel *a* indicate the roots of Eq. (44). The height of peaks in panel *b* represents the relative intensity of the δ -like peaks of $[-\text{Im}\chi(\omega)/\omega]$.

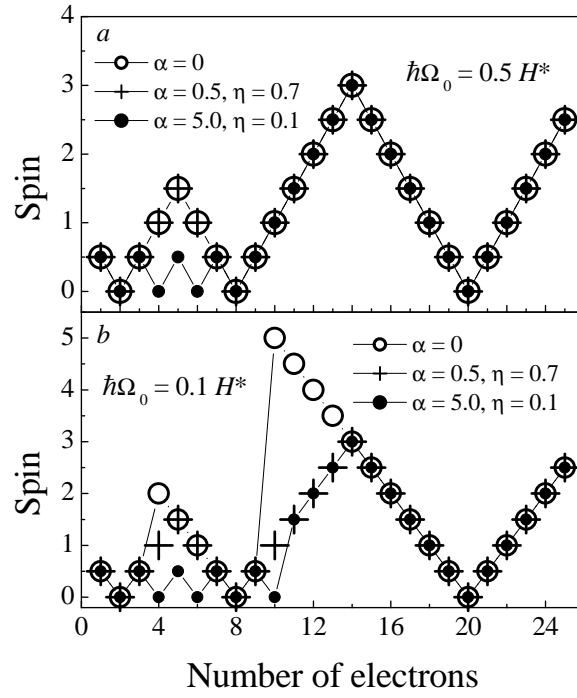


Fig. 1 S. N. Klimin, V. M. Fomin, F. Brosens, J. T. Devreese

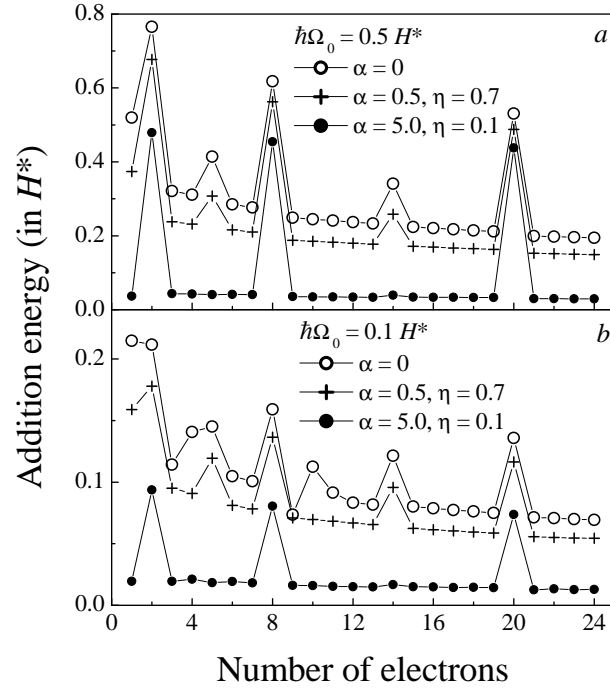


Fig. 2 S. N. Klimin, V. M. Fomin, F. Brosens, J. T. Devreese

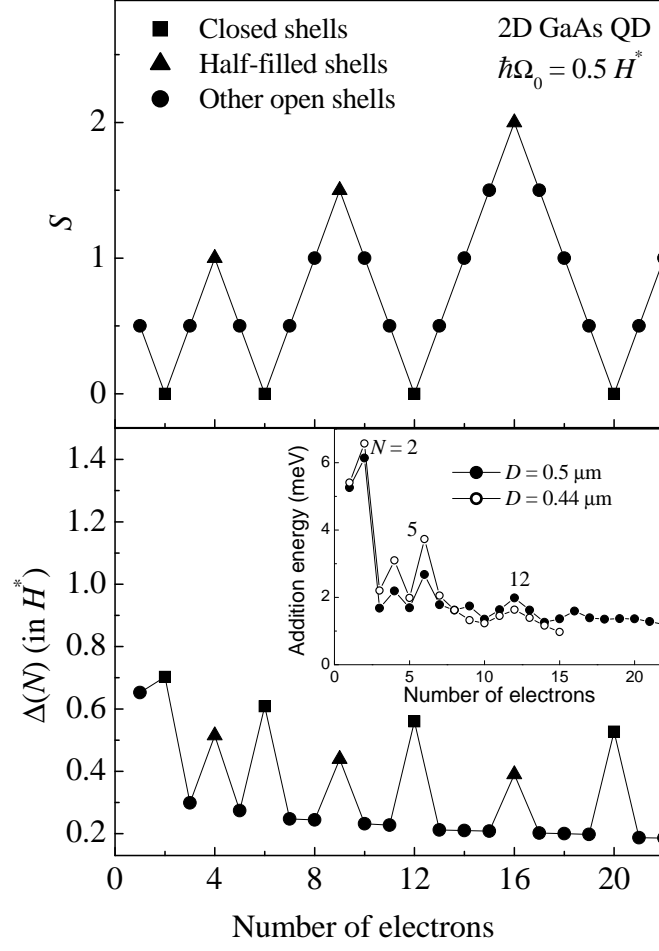


Fig. 3 S. N. Klimin, V. M. Fomin, F. Brosens, J. T. Devreese

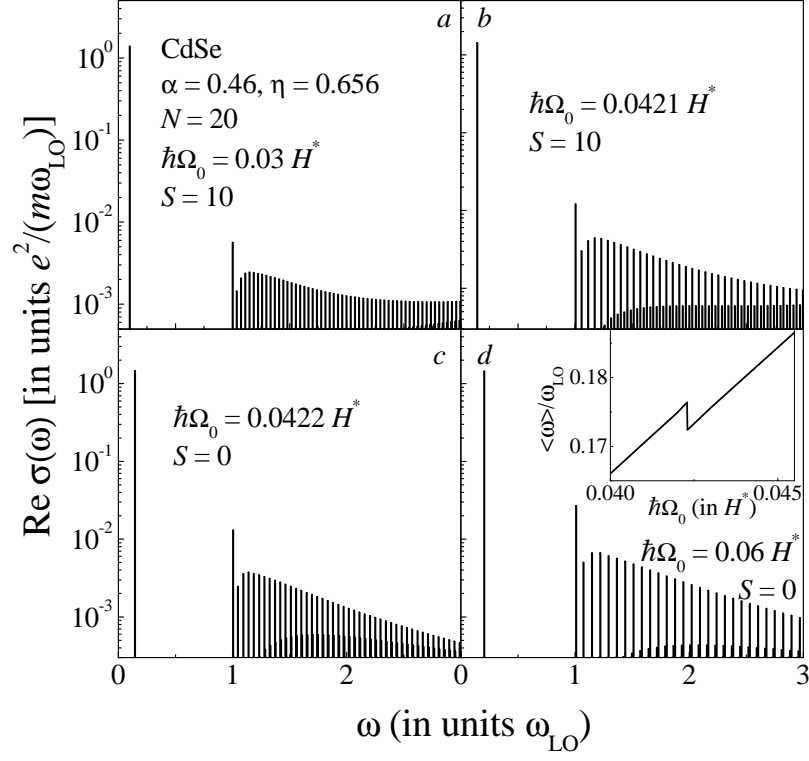


Fig. 4 S. N. Klimin, V. M. Fomin, F. Brosens, J. T. Devreese

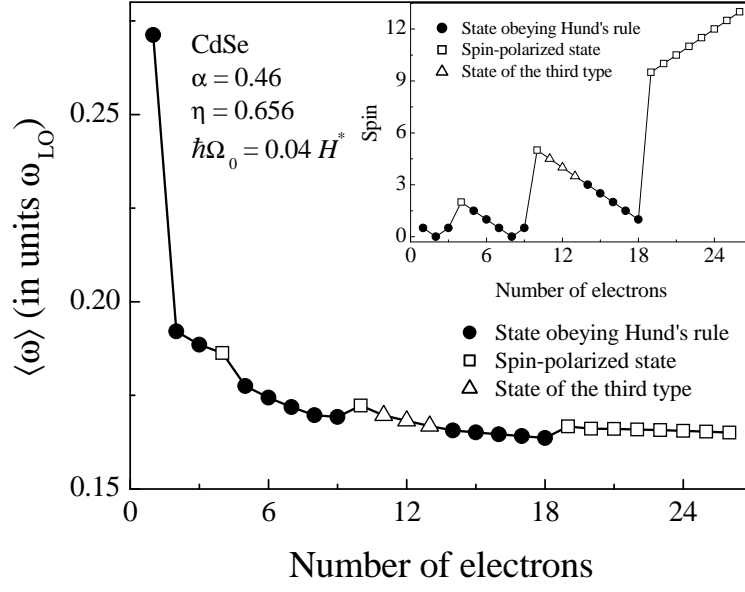


Fig. 5 S. N. Klimin, V. M. Fomin, F. Brosens, J. T. Devreese

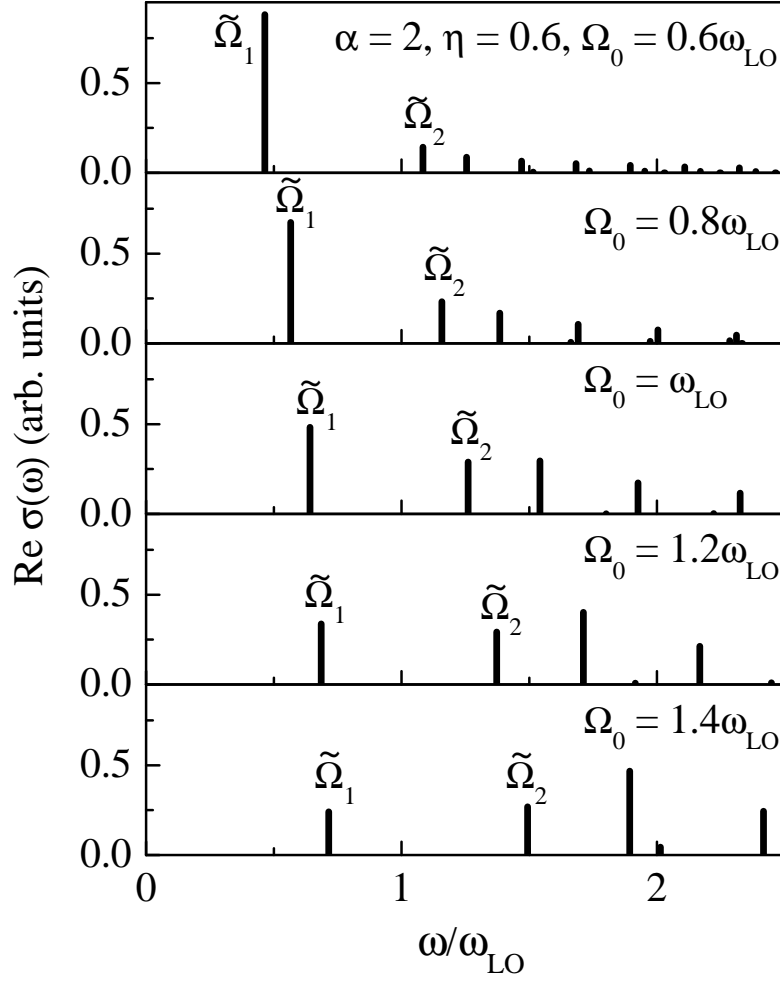


Fig. 6 S. N. Klimin, V. M. Fomin, F. Brosens, J. T. Devreese

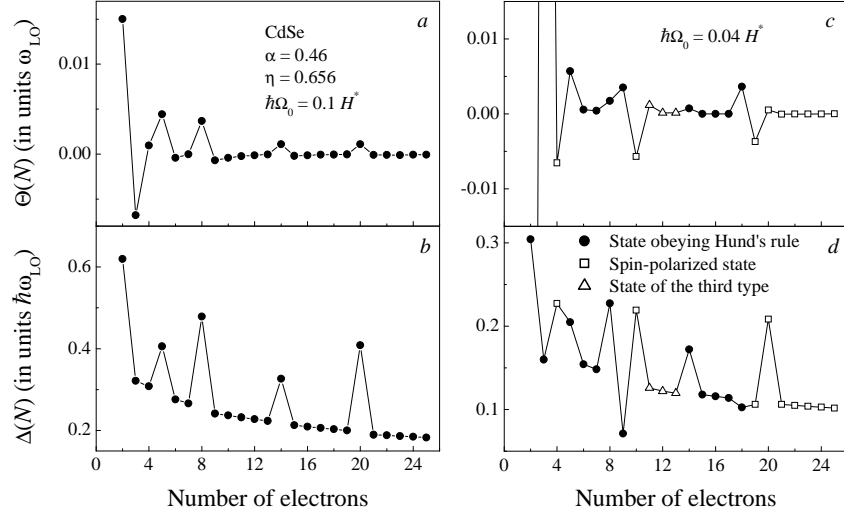


Fig. 7 S. N. Klimin, V. M. Fomin, F. Brosens, J. T. Devreese

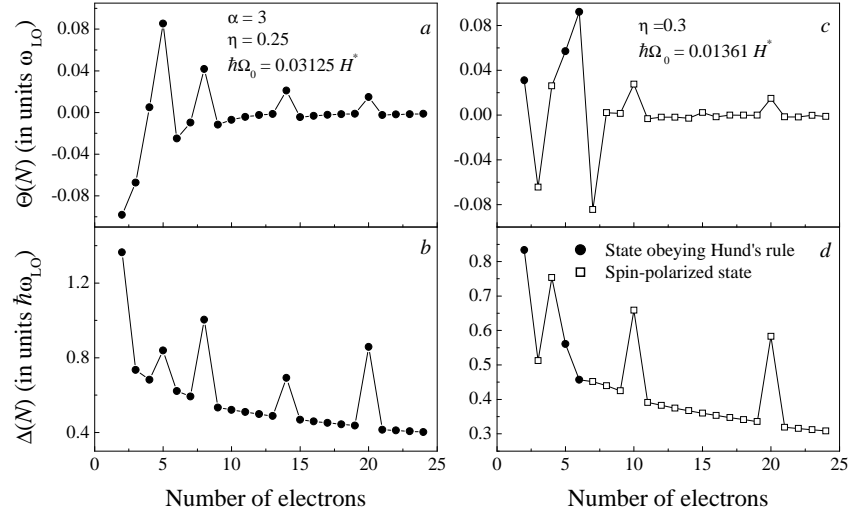


Fig. 8 S. N. Klimin, V. M. Fomin, F. Brosens, J. T. Devreese

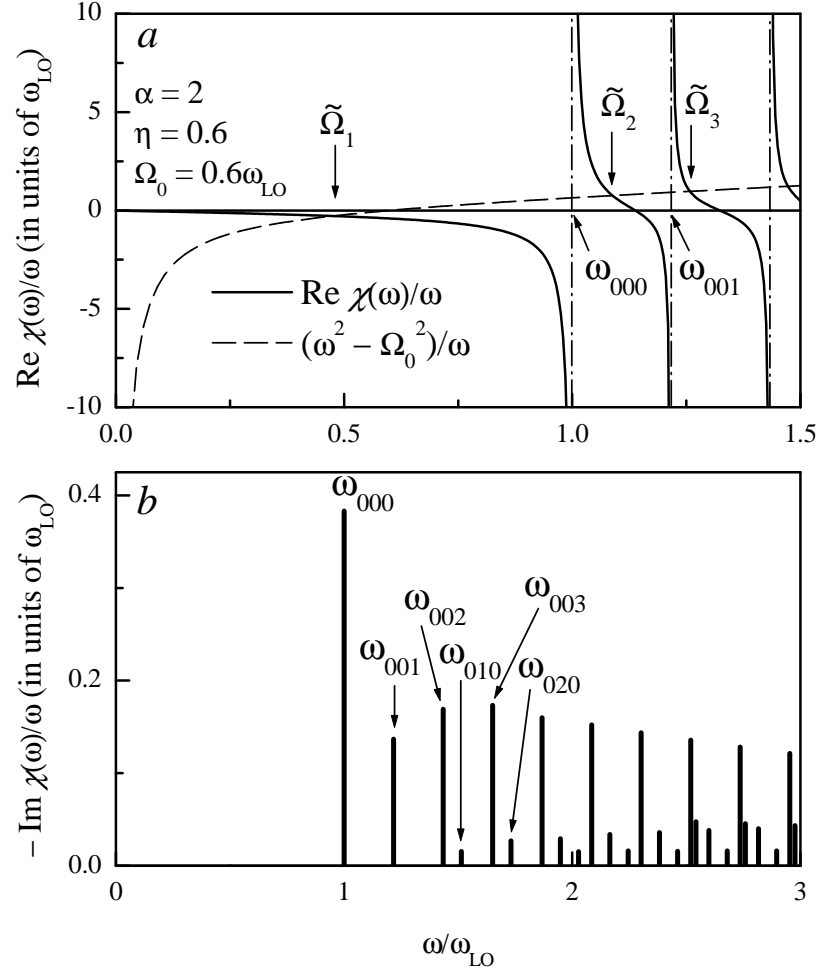


Fig. 9 S. N. Klimin, V. M. Fomin, F. Brosens, J. T. Devreese